AMERICAN JOURNAL OF PHYSIOLOGY
RENAL PHYSIOLOGY

Am J Physiol Renal Physiol 331: F175–F189, 2026.
First published June 27, 2026; doi:10.1152/ajprenal.00001.2026

RESEARCH ARTICLE

Etanercept attenuates TNFα-mediated kidney injury in a rat model of brain death kidney donation

Tiago Pinto Coelho,[1] Jihad Abdelmalki,[1] Margaux Navez,[1] Morgan Vandermeulen,[3,4] Pauline Erpicum,[1,2] Olivier Detry,[3,4] and Francois Jouret[1,2]

[1]*Laboratory of Translational Research in Nephrology – GIGA Institute, Liege University, Liege, Belgium;* [2]*Division of Nephrology, Department of Internal Medicine, University Hospital of Liege, Liege, Belgium;* [3]*Division of Abdominal Surgery and Transplantation, Department of Surgery, University Hospital of Liege, Liege, Belgium; and* [4]*Department of Surgery's Teaching and Research Center – GIGA Institute, Liege University, Liege, Belgium*

Abstract

Brain death (BD) induces a robust inflammatory response that impairs kidney quality before transplantation. Given that TNFα is a central upstream mediator of BD-related injury, we investigated whether selective TNFα inhibition using etanercept could mitigate renal damage in a rat model of BD. BD was maintained for 6 h in anesthetized rats ($n = 6$ controls; $n = 12$ etanercept-treated; balanced for sex), after which animals were randomized to receive either etanercept (ETNCPT) or vehicle (CTL). We evaluated serum biomarkers, histological kidney injury, immune cell infiltration, and whole-kidney transcriptomic profiles. Etanercept significantly reduced circulating TNFα levels (15.25 [12.30–21.05] vs. 34.23 [26.03–50.19] pg/mL; $P < 0.001$), whereas other cytokines remained unchanged. Kidney function parameters [serum creatinine and blood urea nitrogen (BUN)], electrolytes, and hemodynamics were similar across groups. In contrast, etanercept markedly attenuated renal injury, reducing acute tubular necrosis (30.0 [15.0–35.0]% vs. 42.5 [40.0–51.3]%; $P < 0.001$), $CD11b^+$ myeloid infiltration (0.13 [0.11–0.15]% vs. 0.21 [0.19–0.27]%; $P < 0.001$), tubular kidney injury molecule-1 expression (0.04 [0.01–0.08]% vs. 0.17 [0.13–0.18]%; $P < 0.001$), and apoptosis (−69%; $P = 0.036$). Transcriptomic analysis identified 281 differentially expressed genes after TNFα blockade, with strong inhibition of inflammatory and apoptotic pathways including TNF signaling, TNFR1/TNFR2 activation, death receptor signaling, and cytokine storm signaling. Predicted downstream effects included reduced kidney cell death and inflammation. Sex-stratified analyses showed similar directional effects in males and females. In summary, early TNFα blockade after BD selectively neutralizes TNFα, limits immune recruitment, and suppresses injury and inflammatory signaling at cellular and transcriptomic levels. Targeting TNFα during kidney donor management may offer a promising strategy to improve kidney quality before transplantation.

NEW & NOTEWORTHY Brain death (BD) remains a major contributor to kidney injury in deceased donors. In this study, we demonstrate that selective TNFα blockade with etanercept during donor management markedly reduces BD-induced renal damage. Using a rat model of 6-h BD, we show that etanercept selectively neutralizes circulating TNFα without altering hemodynamics or kidney function markers yet significantly decreases tubular injury, myeloid infiltration, KIM-1 expression, and apoptosis. Whole-kidney transcriptomics confirmed broad suppression of TNF-dependent inflammatory and apoptotic pathways. These findings confirm TNFα as a central mediator of BD-associated renal injury and support TNFα-targeted interventions as a promising strategy to improve the quality of BD donor kidney before transplantation.

brain death; kidney donor; TNF-alpha

INTRODUCTION

Kidney transplantation remains the gold-standard treatment for end-stage renal disease, offering superior long-term survival compared with dialysis (1–3). About 90% of transplanted kidneys are procured from deceased donors, with donation after brain death (DBD) historically considered the preferred source due to the preservation of organ perfusion until procurement (4, 5).

Delayed graft function (DGF) is a condition in kidney transplantation where the transplanted kidney does not start working immediately, requiring dialysis within the first week post-transplant (6, 7). Paradoxically, although DBD kidneys exhibit lower rates of initial DGF compared with donation after circulatory death (DCD) kidneys (8), DBD kidneys with DGF demonstrate substantially worse long-term graft survival compared with DCD kidneys with comparable DGF (7, 9–11). This counterintuitive observation suggests that the mechanisms of organ injury initiated by brain death (BD) are fundamentally distinct from those triggered by controlled circulatory arrest, potentially involving more severe and irreversible tissue damage (12).

Correspondence: T. Pinto Coelho (tpintocoelho@uliege.be).
Submitted 5 January 2026 / Revised 19 May 2026 / Accepted 16 June 2026

1931-857X/26 Copyright © 2026 The Authors. Licensed under Creative Commons Attribution CC-BY 4.0.
Published by the American Physiological Society.

Downloaded from journals.physiology.org/journal/ajprenal at Université de Liège (139.165.031.035) on July 14, 2026.

The pathophysiological cascade following brain death encompasses neurohormonal disruption, hemodynamic instability, and widespread systemic inflammation (13, 14). Central to this cascade is the development of a cytokine storm—a systemic inflammatory surge characterized by massive cytokine release (15, 16). Our previous transcriptomic analyses of DBD kidneys established that brain death triggers a pronounced TNFα-driven injury signature characterized by enriched inflammatory and apoptotic signaling pathways. This TNFα-centered injury profile identifies TNFα as a critical mechanistic driver of brain death-induced kidney damage (12). TNFα has been mechanistically implicated in kidney injury through multiple pathways, including promotion of apoptosis via death receptor signaling, induction of myeloid cell infiltration through chemokine upregulation, and activation of inflammatory cascades through TNFR1- and TNFR2-dependent mechanisms (17–20). Selective blockade of TNFα in the DBD donor could therefore preserve graft quality and potentially translate into improved transplant outcomes.

Etanercept is a soluble TNF receptor-immunoglobulin fusion protein, which functions by sequestering TNFα and preventing its interaction with membrane-bound TNF receptors. Etanercept has demonstrated efficacy in attenuating brain death-associated liver injury in experimental transplantation models (21). Furthermore, etanercept has an established safety profile in solid organ transplant recipients for management of inflammatory complications, providing clinical precedent for its application in the transplant setting (22).

The present study investigates in rats whether early administration of etanercept immediately following brain death induction can suppress the TNFα-driven inflammatory cascade in kidneys.

MATERIALS AND METHODS

Brain Death Induction and Animal Management

In this study, inbred male ($n = 9$) and female ($n = 9$) Lewis rats (Charles River Laboratories France, Les-Oncins, France) weighing ~250 g were used. Before enrollment in the study, all animals underwent a minimum acclimatization period of 7 days at ULiege animal facility. The study received approval from the Animal Ethical Committee of Liège University (#2570). The number of animals in each group was calculated taking into account the 3 R rule. Brain death was induced under general anesthesia as previously described (12). Briefly, controlled intracranial hypertension was generated by progressive inflation of a 3 Fr Fogarty balloon catheter positioned in the extradural space via fronto-lateral trepanation. The catheter was inflated at 100 μL/min over 4 min to achieve mechanical brain compression. Brain death was confirmed by the absence of corneal and pupillary reflexes, presence of the Cushing reflex, and a positive 60-s apnea test. Upon confirmation of brain death, animals were randomized to receive either etanercept (Enbrel, Pfizer; 2.4 μg/kg body weight in normal saline; ETNCPT group) or vehicle alone (normal saline; CTL group) via subcutaneous injection in the left flank. Hemodynamic support during the 6-h brain death maintenance period consisted of continuous intravenous normal saline infusion (1 mL/h) with supplemental norepinephrine (Aguettant, France; 20–60 μg/kg/h) as needed to maintain mean arterial pressure ≥ 65 mmHg. Core body temperature was maintained at 38°C using a feedback-controlled heating pad connected to a rectal temperature probe (Fig. 1).

Organ Procurement

Thirty minutes before the time of procurement, a midline laparotomy was made extending from the xiphoid process to the symphysis pubis. Intestinal loops were mobilized to the right and protected with saline-moistened gauze. The infrarenal abdominal aorta was dissected free from surrounding tissues, with ligation of genital vessels and all arterial branches. The suprarenal aorta was similarly mobilized to the level of the celiac trunk, with mesenteric and collateral branches ligated. Systemic heparinization (1,000 U intravenously) was achieved 10 min before vascular clamping. At the moment of procurement, the suprarenal aorta was cross-clamped, immediately followed by cold flush with Institut Georges Lopez 1 (IGL-1) preservation solution (Institut Georges Lopez, France) without any warm ischemic time. Simultaneously, the inferior vena cava was transected to enable venous drainage. The abdominal cavity was filled with slushed ice to allow rapid organ cooling.

Serum Biomarker Quantification

Blood samples were collected into serum separator tubes (BD Microtainer SST, NJ) before brain death induction (baseline) and at the time of organ procurement (6 h post-brain death). Samples were allowed to clot at room temperature for 30 min and then centrifuged at 2,000 *g* for 10 min to obtain serum. Serum concentrations of interleukin-1β (IL-1β), interleukin-10 (IL-10), interleukin-6 (IL-6), and CXCL2 were measured using a multiplexed bead-based immunoassay (Luminex 4-plex assay, Bio-Techne, MN) with twofold sample dilution. Main electrolytes, serum creatinine, and blood urea nitrogen were quantified using enzymatic colorimetric assays on an automated clinical chemistry analyzer (Alinity c; Abbott, IL). Serum tumor necrosis factor-α concentration was determined by enzyme-linked immunosorbent assay (Cat. No. RTA00-1; Bio-Techne) with twofold sample dilution.

Histological Evaluation and Immunohistochemistry

Kidney tissue samples were fixed in 4% neutral-buffered formalin for 24 h and then processed for paraffin embedding using standard protocols. Serial 5-μm sections were prepared for histological and immunohistochemical staining. Periodic acid Schiff staining was performed to evaluate tubular injury. Acute tubular necrosis (ATN) severity was scored in a blinded manner by an experienced renal pathologist using established semiquantitative criteria, with duplicate and averaged independent scoring.

For immunohistochemical detection, deparaffinized sections underwent heat-mediated antigen retrieval. Endogenous peroxidase activity was quenched by incubation with 3% hydrogen peroxide (Cat. No. 107209; Merck) for 20 min at room temperature. Nonspecific antibody binding was blocked using protein block reagent (Cat. No. X0909; Dako) for 10 min. Sections were incubated with primary antibodies against K_i-67, CD11b, caspase-3, and kidney injury molecule-1 (KIM-1) for 60 min at room temperature. For CD68/iNOS and CD68/CD163 costainings, the primary antibodies were applied sequentially, with

Downloaded from journals.physiology.org/journal/ajprenal at Université de Liège (139.165.031.035) on July 14, 2026.

Figure 1. Experimental design and sample collection timeline. After BD induction and confirmation—4 min after induction onset—animals were randomized to receive either etanercept (2.4 mg/kg in normal saline, s.c.) or an equivalent volume of normal saline alone. A first blood sample (red dot) was collected immediately after venous catheter placement, and a second sample was obtained 10 min before aortic clamping. After the cold flush, the left kidney was harvested and transversely bisected: one half was fixed in 4% formalin, whereas the other was snap-frozen in liquid nitrogen and stored at −80°C for histological and molecular analyses, respectively. Serum samples were stored at −80°C until further processing.

each antibody incubated for 60 min at room temperature. Following primary antibody incubation and washing, sections were incubated with appropriate species-matched horseradish peroxidase-conjugated secondary antibodies for 30 min (Table 1). Immunoreactivity was visualized using 3,3′-diaminobenzidine (DAB) chromogen substrate (Cat. No. K3468; Dako) or HIGHDEF Green AP Chromogen substrate (Cat. No. ENZ-ACC130; Enzo). Quantitative analysis of immunostaining was performed in a fully blinded manner with respect to group allocation and outcomes. Histological slides were anonymized and assigned unique identifiers by the histology platform before analysis. These identifiers were used throughout image processing. Images were acquired at ×10 magnification, allowing assessment of the entire corticomedullary transversal section using three non-overlapping fields per kidney. A single fixed threshold was defined using representative images from all samples and applied uniformly to all slides for each staining. Image analysis was performed using ImageJ software (v1.53a; National Institutes of Health) with the Color Deconvolution 2 plugin for separation of DAB and hematoxylin channels. Fully automated ImageJ macros were used for all quantifications to minimize operator-dependent variability. For KIM-1, the DAB-positive area was quantified and expressed as a percentage of the total tissue area defined on the hematoxylin channel. For K_i-67 and CD11b, positive cells were expressed as a percentage of total cell number per field. For caspase-3, the number of tubules containing positive nuclear staining was quantified and normalized to the number of glomeruli per section to exclude basal cytoplasmic procaspase-3 immunoreactivity. Representative images were acquired at ×40 magnification for illustrative purposes.

Transcriptomic Profiling and Bioinformatic Analysis

Kidney tissue samples were snap-frozen in liquid nitrogen immediately following procurement and stored at −80°C until processing. Frozen samples were mechanically disrupted at 2,500 rpm for 20 s using a tissue homogenizer (Mikro-Dismembrator S, Braun Biotek, Germany). Total RNA extraction from 50 mg pulverized tissue was performed using the NucleoZOL reagent followed by column purification with the NucleoSpin RNA Kit (Macherey-Nagel, Düren, Germany) according to the manufacturer's protocol. RNA concentration and purity were quantified by spectrophotometry (NanoDrop Lite; Thermo Scientific, MA), and RNA integrity was assessed using capillary electrophoresis (Fragment Analyzer 5200, Agilent, CA).

Strand-specific cDNA libraries were constructed using the TruSeq Stranded mRNA Library Prep Kit (Illumina, CA) and sequenced on the NovaSeq 6000 platform (Illumina) using paired-end 150 bp reads with S4 flow cell chemistry (NovaSeq S4 V1.5 reagent kit, 300 cycles XP workflow), generating ∼25 million read pairs per sample.

Raw sequencing reads were demultiplexed, and adapter sequences removed using Illumina bcl2fastq conversion software v2.20. Quality control and preprocessing were performed using a custom Nextflow pipeline based on nf-core/rnaseq framework. TrimGalore software was employed to remove single bases from 5′ and 3′ read termini, perform quality-based trimming, and eliminate poly-G tails. Trimmed reads were aligned to the *Rattus norvegicus* reference genome (GRCr8) using STAR aligner, with transcript quantification performed using Salmon software based on Ensembl release 115 annotations. Comprehensive quality assessment was conducted using integrated quality control modules, with results compiled into MultiQC reports.

Differential gene expression analysis was conducted in R (version 4.5.1) using the DESeq2 package (v1.48.2). The experimental design formula (design = ∼ sex + treatment) controlled for sex effects while identifying treatment-responsive genes. To identify robust transcriptional signatures without overinflating gene lists, genes were considered significantly differentially expressed if they exhibited an adjusted P value <

Table 1. *Antibodies used for immunohistochemistry (IHC) analysis*

1°Ab	#Ref	Dilution	Ag Retrieval	2°Ab	#Ref	Dilution
Ki67	#790-4286; Roche	1:2	EDTA (#950-224; Roche)	Env + Anti-Rb HRP	#K4003; Dako	NA
CD11b	#Ab133357; Abcam	1:3,000	TARGET (#S1699; Dako)	Env + Anti-Rb HRP	#K4003; Dako	NA
Casp 3	#NB10056708; R&D	1:100	TARGET (#S1699; Dako)	Env + Anti-Ms HRP	#K4001; Dako	NA
KIM1	#AF3689; R&D	1:50	TARGET (#S1699; Dako)	Poly Anti-Gt HRP	#P0449; Dako	1:400
CD68	#ab125212; Abcam	1:200	EDTA (#950-224; Roche)	Env + Anti-Rb HRP	#K4003; Dako	NA
iNOS	#MAB9502; R&D	1:1,000	EDTA (#950-224; Roche)	Anti-Ms IgG AP	#31320; Invitrogen	1:10,000
CD163	#NBP2-39099; R&D	1:100	EDTA (#950-224; Roche)	Anti-Ms IgG AP	#31320; Invitrogen	1:10,000

Primary antibodies, dilutions, and antigen retrieval methods used for immunohistochemical detection of Ki-67, CD11b, caspase-3 (Casp 3), kidney injury molecule-1 (KIM-1), Cluster of differentiation 68 (CD68), inducible Nitric Oxyde Synthase (iNOS), and Cluster of Differentiation 163 (CD163). Secondary detection employed horseradish peroxidase (HRP)-conjugated anti-rabbit, anti-mouse, or anti-goat antibodies or Alkaline Phosphatase (AP)-conjugated anti-mouse antibody as appropriate. 1°Ab, primary antibody; 2°Ab, secondary antibody; #Ref, catalog number; Ag Retrieval, antigen retrieval method; EDTA, ethylenediaminetetraacetic acid; NA, not applicable; TARGET, proprietary antigen retrieval solution.

Downloaded from journals.physiology.org/journal/ajprenal at Université de Liège (139.165.031.035) on July 14, 2026.

0.05 and a $|\log_2$ fold change$| \geq 0.32$. This inclusive cutoff allowed the detection of modest yet consistent expression changes across multiple genes within specific biological pathways. In a second step, differential expression analyses were conducted separately in males and females, and the resulting gene sets were subjected to comparative gene set enrichment and pathway analyses. The biomaRt package (v2.64.0) facilitated gene annotation and identifier conversion. Principal component analysis visualizations were generated using ggplot2 (v4.0.0) and volcano plots with EnhancedVolcano (v1.26.0).

Pathway enrichment and upstream regulator analyses were performed using QIAGEN Ingenuity Pathway Analysis software (IPA, version 150276282; QIAGEN Inc., https://digitalinsights.qiagen.com/IPA). Only kidneys without macroscopic abnormalities (hematuria, heterogeneous parenchymal perfusion, or inadequate flush) were included in transcriptomic analyses.

Statistical Analysis

Data are presented as medians with interquartile ranges for continuous variables unless otherwise specified. All statistical analyses were performed using GraphPad Prism v. 9.4.0. Animals of both sexes (females and males) were included to assess whether the treatment effect was consistent across sexes. For nontranscriptomic outcomes, a two-way ANOVA was performed with sex and treatment as fixed factors, followed by Šídák's multiple comparisons post-hoc tests. Since no significant sex $\times$ treatment interaction was detected for any variable (all interaction P values > 0.05), indicating that the magnitude and direction of the treatment effect were similar in females and males, the data were presented pooled in the main figures for clarity. The corresponding sex-stratified descriptive statistics and adjusted P values are provided in Tables 2 and 3. Two-way ANOVA results, including the formal assessment of interaction terms, are presented in the Supplemental Table S1. For all analyses, $P < 0.05$ was considered statistically significant.

RESULTS

Biological Parameters Were Stable across Groups, and Kidney Function Parameters Were Not Modified by Etanercept

Mean arterial pressure was similar between ETNCPT (99.3 [91.6–105.5] mmHg) and CTL (100.7 [95.3–102.7] mmHg) animals without group effect ($P = 0.57$), nor time $\times$ group interaction ($P = 0.29$), indicating that blood pressure evolved similarly in both groups (Fig. 2). To assess whether Etanercept has a nephrotoxicity per se, we measured serum creatinine and blood urea nitrogen before brain death induction and at the moment of organ procurement (i.e., 6 h later). The rise of serum creatinine was comparable between etanercept-treated animals ($+0.06$ [0.04–0.07] mg/dL/h) and control animals ($+0.05$ [0.04–0.08] mg/dL/h; $P = 0.62$). Note that SCr remains in the normal range (i.e., 0.5 [0.4–0.7] mg/dL) for all animals. Blood urea nitrogen increase was also comparable between groups (ETNCPT: $+2.81$ [2.16–3.12] mg/dL/h vs. CTL: $+2.55$ [2.07–2.91] mg/dL/h; $P = 0.34$) (Fig. 3, Tables 2 and 3). Electrolytes also showed no significant differences between treated and control animals, nor compared with baseline values, except for chloride levels in females only, which were significantly higher in the etanercept-treated group compared with controls (123.60 [112.60–127.60] vs. 103.40 [100.60–108.10]; $P = 0.05$, respectively) (Table 2).

Etanercept Effectively Neutralizes TNFα

To establish the efficacy of Etanercept in TNFα neutralization, we first measured circulating inflammatory mediators following etanercept administration. Serum TNFα concentration was significantly reduced in etanercept-treated animals (15.25 [12.30–21.05] pg/mL) compared with vehicle-treated controls (34.23 [26.03–50.19] pg/mL; $P = 0.0006$) (Fig. 3). Circulating levels of other proinflammatory mediators, including IL-1β, IL-10, IL-6, and CXCL, were not significantly altered by etanercept treatment within the 6-h observation period (Fig. 3, Table 3).

Table 2. *Kidney function markers and main electrolytes*

	Sex	Baseline	CTL	ETNCPT	*P*
Serum					
SCr (mg/dL)	M	0.31 [0.34–0.40]	0.55 [0.38-0.95]	0.56 [0.51-0.61]	0.999
	F		0.53 [0.46-0.56]	0.52 [0.49-0.56]	0.782
	All		0.54 [0.38-0.66]	0.54 [0.50-0.58]	0.676
BUN (mg/dL)	M	14.79 [12.34–19.51]	28.60 [27.38-33.18]	31.33 [28.62-32.98]	0.906
	F		35.23 [27.21–37.15]	32.18 [28.50-35.11]	0.879
	All		30.89 [27.34–35.71]	31.33 [29.59-34.08]	0.968
Na^+ (mmol/L)	M	155.00 [152.00–165.00]	158.60 [153.60–164.00]	150.70 [148.40–161.10]	0.358
	F		161.50 [157.60–161.80]	162.70 [161.90–167.60]	0.544
	All		160.10 [156.60–162.40]	161.90 [149.70–165.30]	0.839
CL^- (mmol/L)	M	118.00 [115.00–132.00]	124.40 [115.40–133.40]	111.80 [108.30–130.00]	0.431
	F		103.40 [100.60–108.10]	123.60 [112.60–127.60]	**0.049**
	All		111.80 [102.70–126.70]	116.20 [109.00–128.30]	0.347
K^+ (mmol/L)	M	3.20 [2.80–3.70]	2.95 [2.76–3.71]	3.90 [3.44–4.15]	0.168
	F		4.65 [4.00–5.23]	4.07 [3.95–4.56]	0.401
	All		3.86 [2.90–4.80]	4.06 [3.69–4.22]	0.694
Ca^{++} (mmol/L)	M	1.90 [1.40–2.01]	1.86 [1.49–2.29]	2.34 [1.73–2.36]	0.478
	F		2.34 [1.90–2.34]	2.10 [1.92–2.33]	0.930
	All		2.10 [1.77–2.34]	2.22 [1.90–2.35]	0.588

Serum levels of renal function indicators and electrolytes, stratified by sex (M: Male, F: Female) and pooled (All) across experimental conditions: Baseline, Control (CTL), and Etanercept-treated (ETNCPT). Data are presented as median (interquartile range, IQR). *P* values derived from Šídák's post-hoc multiple comparisons test following two-way ANOVA are provided to indicate statistically significant differences between groups ($P < 0.05$). The value in bold indicates statistically significant differences. BUN, blood urea nitrogen.

Downloaded from journals.physiology.org/journal/ajprenal at Université de Liège (139.165.031.035) on July 14, 2026.

Table 3. *Descriptive statistics of serum cytokines, renal function, and histological markers*

	Sex	CTL	ETNCPT	*P*
Serum				
TNFα (pg/mL)	M	26.49 [24.66–35.70]	12.96 [8.16–19.04]	**0.049**
	F	45.49 [32.75–64.28]	18.15 [13.99–23.74]	**<0.001**
	All	34.23 [26.03–50.19]	15.25 [12.30–21.05]	**<0.001**
IL-1β (pg/mL)	M	102.20 [51.04–115.30]	198.60 [104.40–297.50]	0.423
	F	362.00 [180.00–401.60]	286.40 [200.00–508.40]	0.963
	All	147.70 [89.43–371.90]	204.80 [198.60–390.30]	0.256
IL-6 (pg/mL)	M	2,172.00 [1,815.00–4,915.00]	3,666.00 [1,403.00–4,455.00]	>0.999
	F	32,604.00 [19,209.00–49,719.00]	37,436.00 [16,433.00–58,651.00]	0.931
	All	12,062.00 [2,082.00–36,883.00]	8,277.00 [3,666.00–4,868.40]	0.884
IL-10 (pg/mL)	M	225.50 [163.20–436.70]	144.00 [110.90–221.90]	0.482
	F	462.40 [328.00–594.10]	435.80 [333.70–583.60]	0.996
	All	382.40 [209.90–495.50]	294.90 [144.00–493.90]	0.591
CXCL2 (pg/mL)	M	101.30 [27.27–594.80]	59.84 [26.76–345.50]	0.995
	F	1,623.00 [1,504.00–2,497.00]	2,970.00 [1,021.00–4,941.00]	0.419
	All	1,049.00 [82.76–1,841.00]	553.00 [56.73–3,295.00]	>0.999
SCr increase (mg/dL/h)	M	0.06 [0.03–0.06]	0.05 [0.04–0.06]	0.995
	F	0.06 [0.03–0.13]	0.07 [0.05–0.08]	0.914
	All	0.06 [0.03–0.08]	0.06 [0.05–0.07]	0.525
BUN increase (mg/dL/h)	M	3.46 [3.38–4.00]	3.26 [2.34–3.83]	0.678
	F	2.61 [1.40–3.05]	2.33 [1.09–3.03]	0.919
	All	3.22 [2.31–3.60]	2.92 [1.73–3.26]	0.404
Histology				
ATN (% surface)	M	40.00 [40.00–50.00]	30.00 [17.50–30.00]	**0.024**
	F	45.00 [40.00–55.00]	32.50 [15.00–36.25]	**0.020**
	All	42.50 [40.00–51.25]	30.00 [15.00–35.00]	**<0.001**
KIM-1 (% pos area)	M	0.141 [0.094–0.173]	0.010 [0.006–0.013]	**<0.001**
	F	0.174 [0.165–0.185]	0.068 [0.046–0.089]	**<0.001**
	All	0.169 [0.129–0.177]	0.043 [0.010–0.077]	**<0.001**
CD11b (% pos cells)	M	0.21 [0.19–0.28]	0.12 [0.10–0.17]	**0.005**
	F	0.21 [0.18–0.27]	0.13 [0.12–0.15]	**0.008**
	All	0.21 [0.19–0.27]	0.13 [0.11–0.15]	**<0.001**
$CD68^+iNOS^+$ (% double pos cells)	M	0.11 [0.10–0.15]	0.07 [0.05–0.09]	**0.020**
	F	0.13 [0.11–0.15]	0.06 [0.04–0.08]	**0.001**
	All	0.12 [0.11–0.15]	0.07 [0.05–0.08]	**<0.001**
$CD68^+iNOS^+$ (% $CD68^+$ cells)	M	57.00 [55.00–61.00]	57.00 [54.00–59.00]	0.849
	F	58.00 [55.00–60.00]	56.00 [55.00–59.00]	0.812
	All	57.50 [55.00–60.25]	57.00 [55.00–59.75]	0.623
CASP3 (pos tubules/glomeruli)	M	2.52 [2.45–2.68]	0.78 [0.32–1.15]	**<0.001**
	F	2.50 [2.20–2.80]	0.75 [0.28–1.31]	**<0.001**
	All	2.51 [2.39–2.71]	0.78 [0.34–1.10]	**<0.001**
Ki67 (% pos cells)	M	1.36 [1.19–1.68]	1.55 [0.89–1.63]	0.949
	F	1.22 [0.74–1.87]	1.64 [1.04–1.82]	0.750
	All	1.29 [1.08–1.73]	1.55 [0.99–1.74]	0.808

Quantitative profiles for serum biochemistry and renal histological parameters, stratified by sex (M: Male, F: Female) and pooled (All) under control (CTL) and etanercept-treated (ETNCPT) conditions. Data are expressed as median (interquartile range, IQR). *P* values in the final column represent the results of Šídák's post-hoc pairwise comparisons between CTL and ETNCPT groups within each stratification layer following Two-way ANOVA. Values in bold indicate statistically significant differences ($P < 0.05$). BUN, blood urea nitrogen.

TNFα Blockade Reduces Renal Accumulation of Myeloid Cells and Tubular Cell Injury after BD

Periodic acid Schiff-stained kidney sections were examined to assess the extent of acute tubular necrosis (ATN). The median percentage of tubular surface area showing ATN was significantly lower in etanercept-treated kidneys (30.0 [15.0–35.0] %) compared with control kidneys (42.5 [40.0–51.3] %; $P = 0.0003$).

Given the central role of myeloid cell accumulation in mediating ischemic organ injury, we quantified macrophage accumulation in brain death kidneys using immunohistochemical detection of CD11b-positive cells. CD11b-positive cell density was substantially reduced in etanercept-treated kidneys (0.13 [0.11–0.15] %) compared with control kidneys (0.21 [0.19–0.27] %; $P = 0.0003$). To further characterize the infiltrating myeloid cell population, we performed double immunostaining for CD68/iNOS and CD68/CD163. $CD68^+/iNOS^+$ cells represented 57% of total $CD68^+$ cells, with no significant difference between etanercept-treated and control kidneys. However, the proportion of $CD68^+/iNOS^+$ cells was significantly lower in the etanercept-treated group compared with controls (0.07 [0.05–0.08] % vs. 0.12 [0.11–0.15] %, respectively; $P < 0.001$). In contrast, $CD68^+/CD163^+$ cells were very scarce, with only a few positive cells detected per analyzed field, precluding any objective comparison between treated and untreated groups.

Markers of tubular epithelial damage were markedly attenuated by etanercept treatment. Kidney Injury Molecule-1 (KIM-1), a highly sensitive and specific biomarker of proximal tubular epithelial cell injury, was substantially reduced in etanercept-treated kidneys (0.04 [0.01–0.08] %) compared with control kidneys (0.17 [0.13–0.18] %; $P = 0.0002$).

To assess the extent of programmed cell death, we quantified caspase-3-positive tubules. After normalization per glomeruli,

Downloaded from journals.physiology.org/journal/ajprenal at Université de Liège (139.165.031.035) on July 14, 2026.

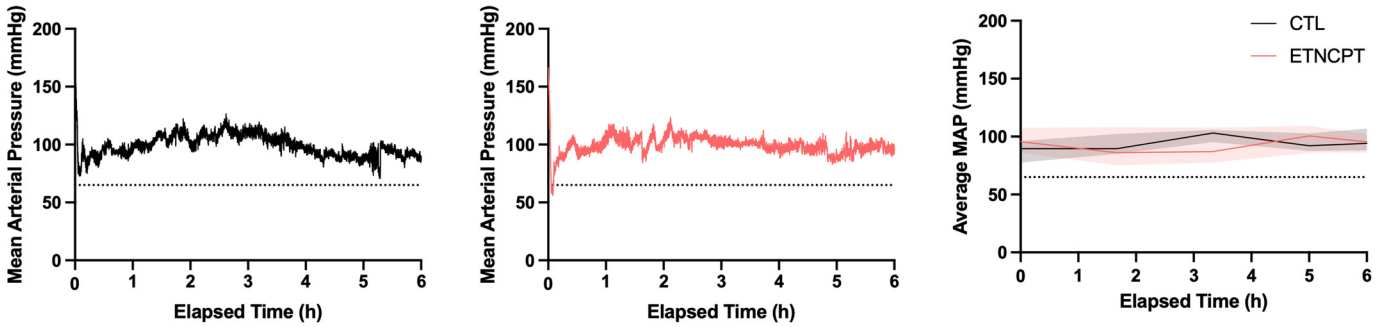

Figure 2. Hemodynamic stability in ETNCPT and CTL rats. Mean arterial pressure (MAP) was continuously monitored over the 6-h observation period. The Cushing reflex (transient MAP elevation) was observed in both CTL and ETNCPT groups at T = 0 h. Shaded areas indicate the median [IQR] for each group. Mean MAP remained comparable between groups and stable over time (no time × group interaction, $P = 0.45$; two-way ANOVA). CTL, control; ETNCPT, etanercept; IQR, interquartile range.

Caspase-3-positive tubules were significantly reduced in etanercept-treated kidneys (0.78 [0.34–1.10] positive tubules/glomeruli) compared with controls (2.51 [2.39–2.71] positive tubule/glomeruli; $P = 0.0002$) (Fig. 4, Table 3).

Principal Component Analysis Revealed Distinct Transcriptomic Patterns in Etanercept-Treated Versus Untreated DBD Kidneys

Principal component analysis (PCA) performed on the whole-kidney transcriptomes from all samples combining males and females revealed that the dominant source of variation (PC1) corresponded exclusively to sex. This strong sexual dimorphism entirely structured the global clustering, with male and female kidneys forming two well-defined groups. In contrast, no discernible separation between control and etanercept-treated samples was observed, indicating that treatment-associated transcriptional changes were largely overshadowed by the magnitude of sex-driven variability. To overcome this confounding effect, we next conducted PCA after stratifying samples by sex. Once males and females were analyzed separately, treatment-related differences emerged: within each sex-specific subset, control and

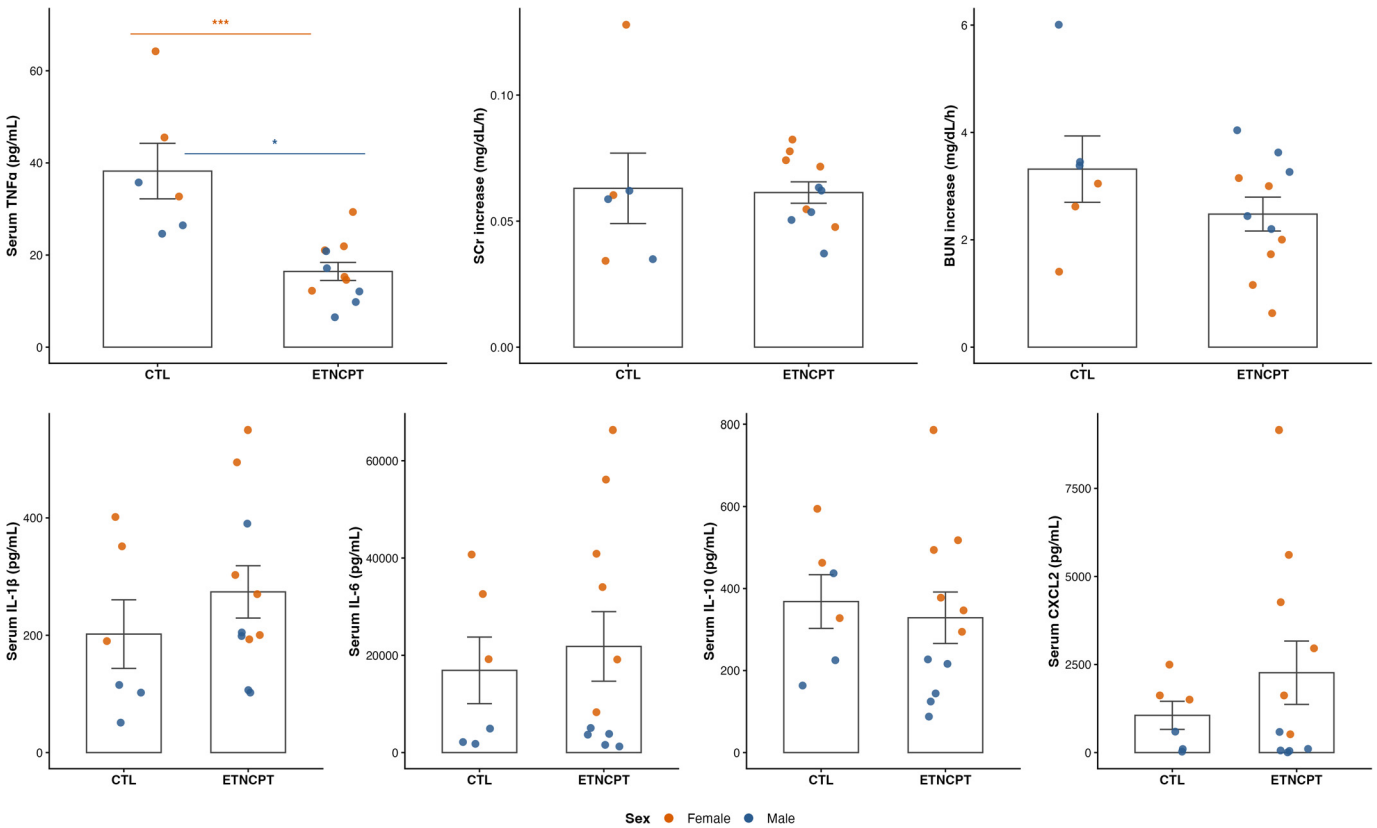

Figure 3. Impact of ETNCPT treatment on serum cytokines and renal function parameters. Serum levels of primary cytokines and indicators of renal function in male (blue dots) and female (orange dots) under control (CTL) and treated (ETNCPT) conditions. Data are expressed as median [IQR] with individual data points displayed. Statistical significance was determined using a two-way ANOVA (with sex and treatment as factors) followed by Šídák's post-hoc test for multiple comparisons (*$P < 0.05$; ***$P < 0.001$). ETNCPT, etanercept; IQR, interquartile range.

Downloaded from journals.physiology.org/journal/ajprenal at Université de Liège (139.165.031.035) on July 14, 2026.

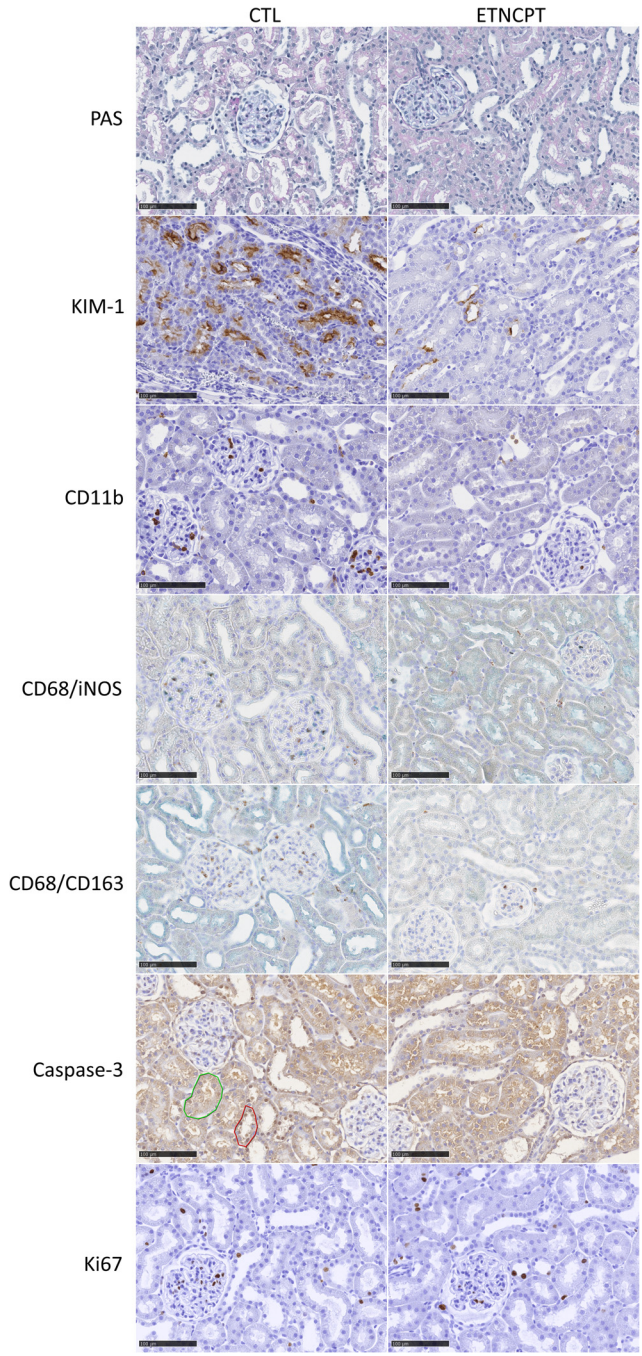

Figure 4. Histological and immunohistochemical evaluation of renal tissue following ETNCPT treatment. Representative micrographs (×40 magnification) of kidney sections from control (CTL) and treated (ETNCPT) groups. (PAS) Periodic Acid-Schiff staining evaluating general tubular morphology and brush border integrity. (KIM-1) Immunohistochemical detection of Kidney Injury Molecule-1 as a marker of proximal tubular injury. (CD11b) Staining of myeloid infiltrating cells. (CD68/iNOS) Double staining for M1-like macrophage polarization profiles; brown color indicates $CD68^+$ only, blue indicates $iNOS^+$ only, and black indicates $CD68^+iNOS^+$ colocalization. (CD68/CD163) Double staining for M2-like macrophage profiles; brown color indicates $CD68^+$ only, blue indicates $CD163^+$ only, and black indicates $CD68^+/CD163^+$ co-localization. (Caspase-3) Evaluation of apoptotic pathways; green outlines indicate low diffuse cytoplasmic staining of pro-caspase 3, whereas red outlines highlight intense nuclear staining of cleaved active caspase-3. (Ki67) Immunohistochemical staining for cellular proliferation. Scale bars = 100 μm. ETNCPT, etanercept.

etanercept-treated kidneys segregated along PC2, revealing consistent and reproducible transcriptional signatures associated with etanercept exposure (Fig. 5).

Differential expression analysis was performed to compare gene expression profiles between etanercept-treated and control animals while accounting for the effect of sex. Using this approach, 281 significantly differentially expressed genes (DEGs) were identified between etanercept-treated and vehicle-treated animals (adjusted P value < 0.05, $|\log_2$ fold change$| \geq 0.32$). Of these 281 DEGs, 159 genes (56.6%) were downregulated and 122 genes (43.4%) were upregulated following etanercept treatment, reflecting comprehensive transcriptional remodeling following TNFα blockade (Fig. 6).

To determine the functional significance of these transcriptional changes, ingenuity pathway analysis was performed on the DEGs. IPA canonical pathway analysis identified 140 significantly enriched pathways in etanercept-treated versus control DBD kidneys. TNF signaling emerged as the most significantly modulated pathway ($P = 2.55 \times 10^{-13}$, z-score $= -1.73$, 21.1% pathway overlap), with upstream regulators including TNF ($P = 3.30 \times 10^{-17}$), IL1B, NFKBIA, and IKBKB showing significant downregulation. Additional TNF-related signaling cascades were significantly suppressed, including TNFR1 signaling (z-score $= -2.45$, $P = 3.72 \times 10^{-8}$) and TNFR2 signaling (z-score $= -2.00$, $P = 2.61 \times 10^{-8}$). Inflammation and immune activation pathways, including Cytokine Storm signaling (z-score $= -3.00$, $P = 1.80 \times 10^{-8}$), Wound Healing signaling (z-score $= -2.32$, $P = 1.60 \times 10^{-8}$), and Macrophage Classical Activation signaling (z-score $= -2.83$, $P = 6.50 \times 10^{-5}$) were significantly inhibited. Cell death pathways including induction of apoptosis (z-score $= -2.65$, $P = 2.50 \times 10^{-7}$), necroptosis signaling (z-score $= -1.67$, $P = 2.80 \times 10^{-6}$), immunogenic cell death signaling (z-score $= -2.65$, $P = 2.10 \times 10^{-6}$), caspase activation (z-score $= -2.00$, $P = 1.40 \times 10^{-5}$), and pyroptosis signaling (z-score $= -2.45$, $P = 4.30 \times 10^{-4}$) were markedly attenuated (Fig. 7*A*, Table 4). At the disease and biological function level, etanercept treatment suppressed both general injury and kidney-specific pathways. Broad categories including organismal injury and abnormalities, inflammatory response, and cell cycle progression were markedly downregulated (z-scores ranging from -1.03 to -3.70, $P < 0.001$). IPA toxicological analysis revealed kidney-specific protective effects focused on three critical renal injury mechanisms. Cell death of kidney cells ($P = 1.85 \times 10^{-5}$, $z = -2.59$) was most significantly suppressed, accompanied by reduced apoptosis across mesangial ($z = -1.96$), glomerular ($z = -1.53$), and kidney cell lines ($z = -1.31$). Proliferation of mesangial cells ($P = 2.6 \times 10^{-6}$, $z = -2.75$) was the most dramatically inhibited renal function. Nephritis was also significantly reduced ($P = 2.46 \times 10^{-3}$, $z = -1.29$).

Immune and hematological responses were comprehensively suppressed. Lymphocyte proliferation ($z = -2.732$) and mononuclear leukocyte proliferation ($z = -2.59$) were significantly inhibited, alongside reduced cell movement of mononuclear leukocytes ($z = -2.54$), leukocyte activation ($z = -2.23$), and lymphopoiesis/leukopoiesis ($z = -1.57$ each). These data suggest that etanercept suppresses kidney injury through simultaneous inhibition of apoptotic cascades, maladaptive proliferative responses, and immune cell trafficking (Fig. 7*A*).

Downloaded from journals.physiology.org/journal/ajprenal at Université de Liège (139.165.031.035) on July 14, 2026.

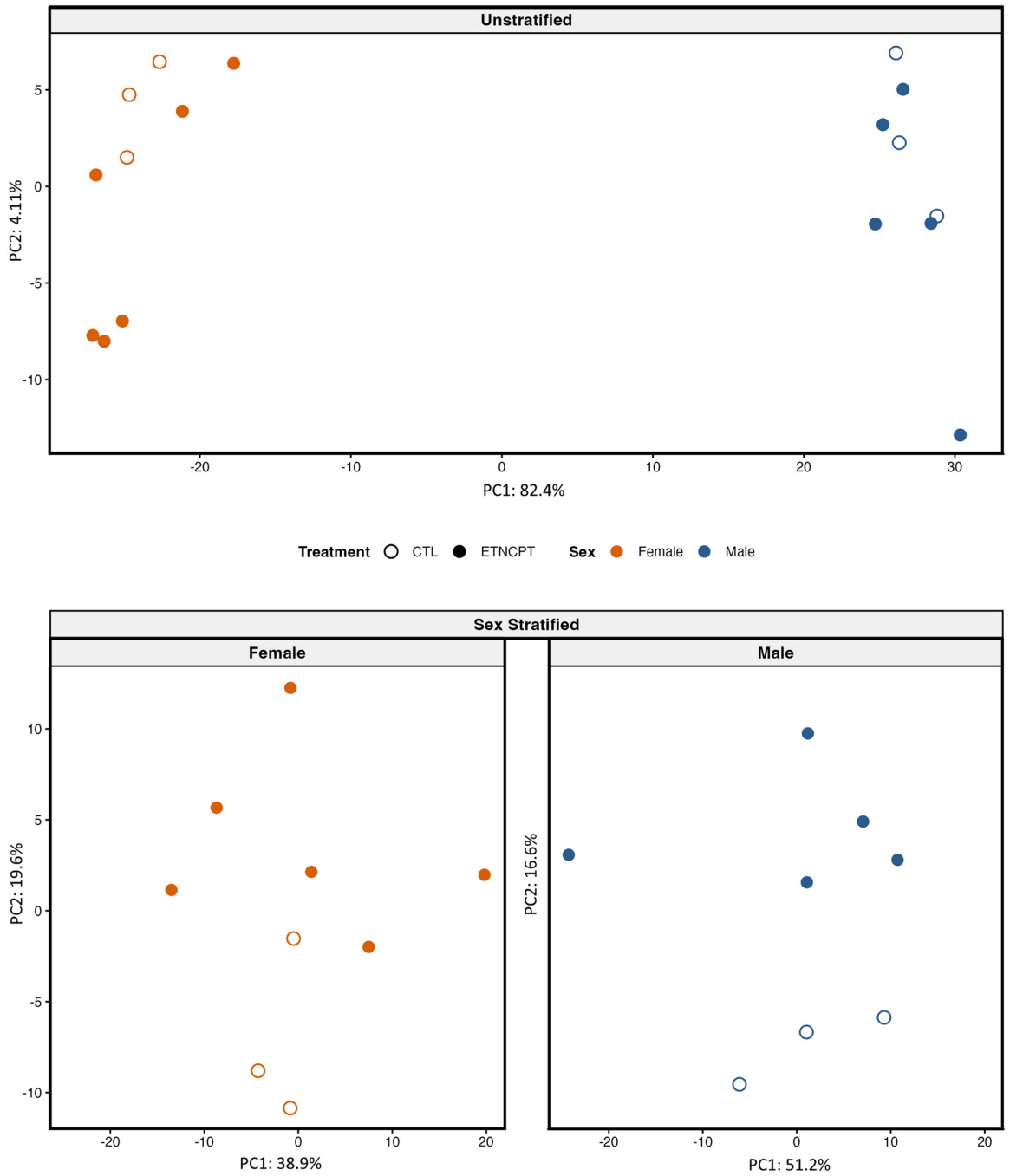

Figure 5. Principal component analysis (PCA) score plots of the experimental groups. The multivariate data distribution is displayed across the first two principal components (PC1 and PC2). *Top*: unstratified PCA plot including all animals. PC1 explains 82.4% of the total variance, predominantly driving the separation between female (orange symbols) and male (blue symbols). *Bottom*: sex-stratified PCA score plots evaluating the impact of treatment within female (*left*) and male (*right*) subgroups independently. Circular shapes indicate the experimental groups: open circles represent control subjects (CTL) and filled circles represent treated animals (ETNCPT). ETNCPT, etanercept.

Causal network analysis identified TNF as a central upstream regulator of 65 genes. Comparison of this gene set with TNF downstream targets identified in our previous work (12) revealed an overlap of 45 genes between both datasets. Notably, these shared genes displayed predominantly opposite expression patterns between conditions, with inverse $|\log_2$ fold changes$|$ observed in DBD versus control (CTL) and etanercept-treated DBD (ETNCPT) versus CTL (Fig. 8).

Sex-Stratified Pathway Analysis Revealed Consistent Directional Effects of Etanercept across Males and Females

To assess whether the protective effects of etanercept were sex-dependent, we performed a comparative enrichment analysis in IPA between separate gene set enrichments for male and female rats. Among the top canonical pathways and disease/biological functions, etanercept-induced suppression was directionally consistent between sexes, with

Downloaded from journals.physiology.org/journal/ajprenal at Université de Liège (139.165.031.035) on July 14, 2026.

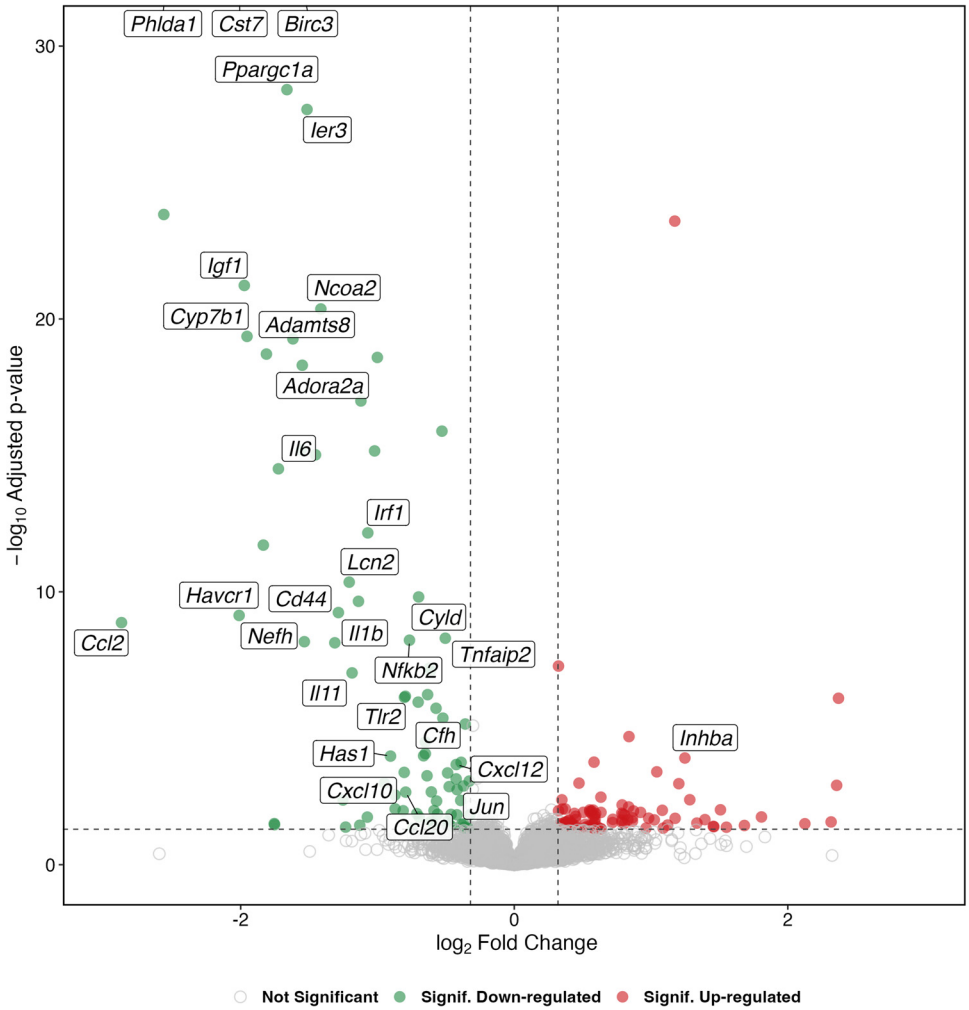

Figure 6. Comparative transcriptomic analysis of ETNCPT and CTL kidney grafts. Volcano plot showing 281 significantly differentially expressed genes (DEGs; adjusted $P < 0.05$, $|\log_2 FC| \geq 0.32$) between etanercept-treated and control donors, including 159 downregulated and 122 upregulated genes. CTL, control; ETNCPT, etanercept.

both males and females demonstrating inhibition of TNF signaling, death receptor signaling, inflammatory amplification pathways, and cell death/survival functions. However, the amplitude of pathway modulation was quantitatively greater in males compared with females (Fig. 7*B*).

DISCUSSION

Kidney transplant research has historically concentrated on recipient-level interventions—including immunosuppressive strategies, induction therapy optimization, and management of calcineurin inhibitor toxicity and on organ-level preservation technologies during the procurement-to-transplant interval (23–29). Normothermic machine perfusion and hypothermic machine perfusion have emerged as promising preservation strategies that extend organ viability and enable objective assessment of graft quality before transplantation (30–32). This study proposes a paradigm shift to the donor side immediately following brain death declaration, before tissue injury. This donor-directed approach complements rather than replaces existing recipient- and preservation-focused strategies, providing a novel opportunity to improve organ quality.

In our previous work, we showed that DBD kidneys harbor a robust TNFα-enriched inflammatory signature, reflecting heightened death receptor signaling, caspase activation, and extensive apoptotic cascades, which may contribute to graft injury and dysfunction. Our transcriptomic analysis predicted TNFα as a central mechanistic driver of brain death-induced kidney damage (12). Accordingly, this pathophysiological characterization provided the mechanistic foundation for the hypothesis that selective TNFα inhibition could specifically reverse the injury signature of DBD donors. The present study provides strong evidence supporting this targeted approach. Etanercept administration at the time of brain death induction resulted in a reduction in serum TNFα levels. Critically, this TNFα reduction was accompanied by preservation of other circulating cytokines (IL-1β, IL-10, IL-6, and CXCL2), demonstrating selectivity of TNFα blockade rather than a broad suppression of innate immunity. Although previous studies in chronic inflammatory diseases have reported increased circulating TNF levels during etanercept therapy, this phenomenon is largely attributed to the formation of stable TNF-etanercept complexes and assay-dependent detection of bound cytokine, particularly in settings with delayed sampling and prolonged drug exposure (33, 34). In contrast, in acute experimental settings with early sampling after administration, TNF levels have been shown to decrease, reflecting rapid ligand binding and functional neutralization. Our findings are consistent with this latter paradigm and were obtained in an acute model using a rat-specific TNF-Quantikine ELISA,

Downloaded from journals.physiology.org/journal/ajprenal at Université de Liège (139.165.031.035) on July 14, 2026.

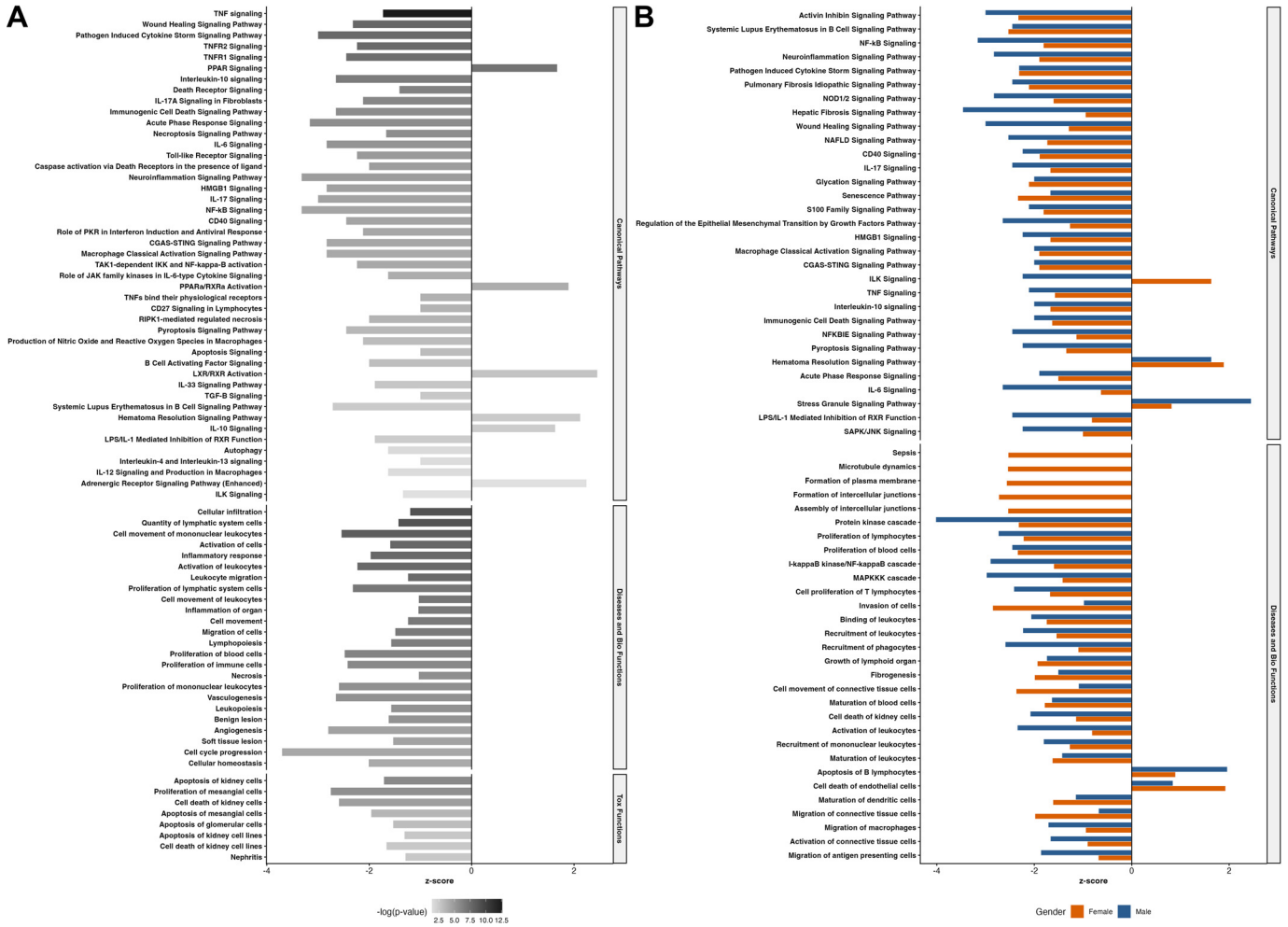

Figure 7. Ingenuity pathway analysis (IPA) of differentially expressed genes. *A*: IPA visualization of pathway modulation following etanercept treatment. Canonical pathways: TNF signaling, cytokine-mediated inflammatory cascades, and cell death mechanisms were significantly inhibited (negative *z*-scores). Diseases and biological functions: immune cell infiltration, leukocyte trafficking, lymphocyte proliferation, and cell cycle progression were markedly downregulated. Renal toxicity functions: apoptosis, cell death, and proliferation of kidney and mesangial cells—as well as nephritis—were substantially reduced. *B*: IPA comparative enrichment analysis of male-specific and female-specific gene sets demonstrated directionally concordant suppression of TNF signaling, death receptor signaling, inflammatory amplification pathways, and cell death/survival functions in both sexes. However, the magnitude of pathway inhibition was greater in males than in females (higher *z*-scores).

with standardized early time point sampling after brain death induction. In this context, the observed reduction in measurable TNFα likely reflects immediate target engagement and sequestration by the soluble TNF receptor fusion protein. Taken together, these data support effective and selective TNFα pathway inhibition in brain-dead donor kidneys (21, 35). Although TNFα, IL-1β, and IL-6 are often co-expressed in acute inflammatory states, they are not exclusively interdependent and display distinct regulatory kinetics (36–40). TNFα has the shortest serum half-life (~15–20 min) and peaks early (2–4 h post-brain death), whereas IL-6 demonstrates a substantially longer half-life (45–60 min) and continues to be produced by multiple cell types—including fibroblasts, endothelial cells, and activated B cells—through TNF-independent mechanisms (37, 41–46). Similarly, IL-1β is primarily regulated through inflammasome-mediated activation and caspase-1 processing, pathways that maintain significant TNF independence (47, 48). Although TNFα enhances IL-6 and IL-1β production through NF-κB and MAPK activation, both cytokines preserve robust production through alternative TNF-independent pathways (49–51). IL-10, the prototypical anti-inflammatory cytokine, can be induced by TNFα through delayed autocrine IL-10/STAT3 signaling. Yet, IL-10 production is maintained through multiple TNF-independent pathways (52–54).

Our transcriptomic and cellular findings converge on a mechanistic explanation for the protective effects of etanercept against brain death-induced kidney injury. At the cellular level, etanercept suppressed caspase-3-positive apoptotic structures by 69% and reduced KIM-1 expression by 74.4%—consistent with robust prevention of tubular epithelial damage. These substantial reductions directly align with the transcriptomic signature revealed by ingenuity pathway analysis, which identified TNF signaling as the most significantly suppressed pathway after exposure to etanercept. This analysis demonstrated significant suppression of TNFR1 signaling, TNFR2 signaling, death receptor signaling pathways, and caspase activation via death receptors.

Downloaded from journals.physiology.org/journal/ajprenal at Université de Liège (139.165.031.035) on July 14, 2026.

Table 4. *Ingenuity pathway analysis of differentially expressed genes in etanercept-treated brain-dead donor kidneys*

	Canonical Pathways	*P* Value	*z*-Score	Genes
Cytokine signaling	TNF signaling	2.5×10^{-13}	−1.73	Casp8, Cflar, Cyld, Map3k7, Sharpin, Tab3, Tax1bp1, Tnfaip3, Tnfrsf1a, Tradd, Traf1, Traf2
	TNFR1/2 signaling	3.7×10^{-8}	−2.44	Birc3, Casp8, Jun, Nfkb2, Tnfaip3, Tnfrsf1a, Tradd, Traf2, Tnfrsf1b, Traf1
	IL6 signaling	4.7×10^{-6}	−2.83	Il1b, Il6, Jun, Map3k7, Nfkb2, Rasd1, Tnfrsf1a, Tnfrsf1b, Traf2
	HMGB1 signaling	2.7×10^{-5}	−2.83	Il11, Il1b, Il6, Jun, Nfkb2, Rasd1, Tgfb3, Tnfrsf1a, Tnfrsf1b
	IL17 signaling	3.5×10^{-5}	−3.00	Ccl20, Il11, Il1b, Il6, Jun, Map3k7, Rasd1, Tgfb3, Traf2
	IL10 signaling	3.7×10^{-3}	1.63	Creb3l3, Il1b, Il6, Jun, Map3k7, Nfkb2
Inflammation and immune activation	Pathogen-induced cytokine storm signaling pathway	1.8×10^{-8}	−3.00	Casp8, Ccl2, Ccl20, Cxcl10, Cxcl12, Cxcl17, Il11, Il1b, Il6, Irf1, Jun, Nfkb2, Pf4, Tgfb3, Tlr2, Tnfrsf1a, Tnfrsf1b, Tradd
	Wound healing signaling pathway	1.6×10^{-8}	−2.32	Acta2, Il11, Il1b, Il6, Jun, Map3k7, Nfkb2, Pdgfd, Pf4, Rasd1, Tgfb3, Tnfrsf1a, Tnfrsf1b, Tradd, Traf2
	Immunogenic cell death signaling pathway	2.1×10^{-6}	−2.65	Casp8, Cflar, Cxcl10, Il1b, Il6, Nfkb2, Tnfrsf1a, Tnfrsf1b
	Macrophage classical activation signaling pathway	6.5×10^{-5}	−2.83	Ccl20, Cxcl10, Il11, Il1b, Il6, Irf1, Map3k7, Nfkb2, Tgfb3
	CD40 signaling	4.5×10^{-5}	−2.45	Jun, Map3k7, Nfkb2, Tnfaip3, Traf1, Traf2
Cell death	Induction of apoptosis by HIV1	2.5×10^{-7}	−2.65	Birc3, Casp8, Nfkb2, Tnfrsf1a, Tnfrsf1b, Tradd, Traf1, Traf2
	Necroptosis signaling pathway	2.8×10^{-6}	−1.67	Birc3, Casp8, Cflar, Cyld, Map3k7, Sharpin, Tnfrsf1a, Tnfrsf1b, Tradd, Traf2
	Immunogenic cell death signaling pathway	2.1×10^{-6}	−2.65	Casp8, Cflar, Cxcl10, Il1b, Il6, Nfkb2, Tnfrsf1a, Tnfrsf1b
	Caspase activation via death receptors in the presence of ligand	1.4×10^{-5}	−2.00	Casp8, Cflar, Tradd, Traf2
	Pyroptosis signaling pathway	4.3×10^{-4}	−2.45	Casp8, Il1b, Nfkb2, Tlr2, Tnfrsf1a, Tnfrsf1b
Metabolism	PPAR signaling	7.2×10^{-8}	1.67	Il1b, Jun, Map3k7, Nfkb2, Pdgfd, Ppargc1a, Rasd1, Tnfrsf1a, Tnfrsf1b, Traf2
	PPARò±/RXRò± activation	1.1×10^{-4}	1.89	Cyp2c65, Cyp2c66, Il1b, Il6, Jun, Map3k7, Nfkb2, Ppargc1a, Rasd1, Tgfb3
	LXR/RXR activation	1.4×10^{-3}	2.45	Alb, Il1b, Il6, Nfkb2, Tnfrsf1a, Tnfrsf1b

Canonical pathway analysis identifying 119 significantly enriched pathways modulated by etanercept treatment (adjusted P value $<$ 0.05). The table lists representative pathways organized by functional category, ranked by P value significance. TNF signaling emerged as the most significantly suppressed pathway ($P = 2.55 \times 10^{-13}$, z-score $= -1.73$), followed by TNFR1/2 signaling, IL-6 signaling, and inflammatory amplification pathways. Cell death pathways including apoptosis induction, necroptosis, and pyroptosis signaling were markedly inhibited (z-scores ranging from -1.67 to -2.65). Metabolic pathways including PPAR signaling and LXR/RXR activation showed activation status (positive z-scores), indicating metabolic adaptations concurrent with inflammatory suppression. Negative z-scores indicate pathway inhibition; positive z-scores indicate pathway activation. Genes listed represent key molecular regulators identified within each pathway. P value calculated by ingenuity pathway analysis; z-score reflects predicted pathway activation state ($z < -2$ or $z > +2$ indicates significant regulation).

TNFα mediates pro-apoptotic signaling through both TNFR1 and TNFR2, with TNFR1 predominantly triggering the extrinsic apoptotic pathway through TRADD recruitment and caspase-8 activation (55, 56). Our transcriptomic findings confirm functional suppression of these pathways at the gene expression level. Notably, CFLAR (c-FLIP), a potent inhibitor of DISC-mediated caspase-8 activation, emerged as a key modulated gene within the TNF signaling pathway, suggesting that etanercept enhances intrinsic anti-apoptotic signaling in addition to reducing TNFR ligation (56–58). Furthermore, upstream regulator analysis identified TNF itself ($P = 3.30 \times 10^{-17}$) along with IL1B, NFKBIA, and IKBKB as significantly downregulated following etanercept treatment. This multi-tiered anti-apoptotic effect—combining direct TNFR inhibition, enhanced anti-apoptotic gene expression, and suppression of downstream signaling intermediates—likely explains the better histopathological preservation of tubular architecture, with acute tubular necrosis reduced from 40% in controls to 30% in etanercept-treated kidneys.

The clinical significance of TNFα-driven injury in kidney transplantation is underscored by recent human genetic evidence. Population-based analysis of TNF polymorphisms demonstrated that donors carrying the high-producing TNFα rs3093662 G-allele exhibited a 58% increased relative risk of late graft loss and doubled risk of primary nonfunction (59). These observations are further supported by recent clinical data from Fawaz et al. who showed in a cohort of 630 human donors across multiple centers in the UK that elevated donor TNF levels were associated with impaired graft function at 12 mo and reduced graft survival at 96 mo (60). Together, these findings support our mechanistic observation that elevated TNFα is a critical risk factor for graft failure. Our demonstration that etanercept suppresses TNFα-driven apoptotic pathways in DBD kidneys provides experimental support for the clinical hypothesis that TNFα blockade could ameliorate outcomes of DBD grafts.

A secondary but biologically significant finding was the reduction in CD11b-positive myeloid cell and CD68/iNOS double-positive cell infiltration, suggesting the suppression of TNFα-dependent chemotaxis and leukocyte recruitment (61–63), without a significant modification of the $CD68^+iNOS^+$/$CD68^+CD163^+$ ratio. Notably, $CD163^+$ cells were rare in both control and treated groups, limiting robust quantitative

Downloaded from journals.physiology.org/journal/ajprenal at Université de Liège (139.165.031.035) on July 14, 2026.

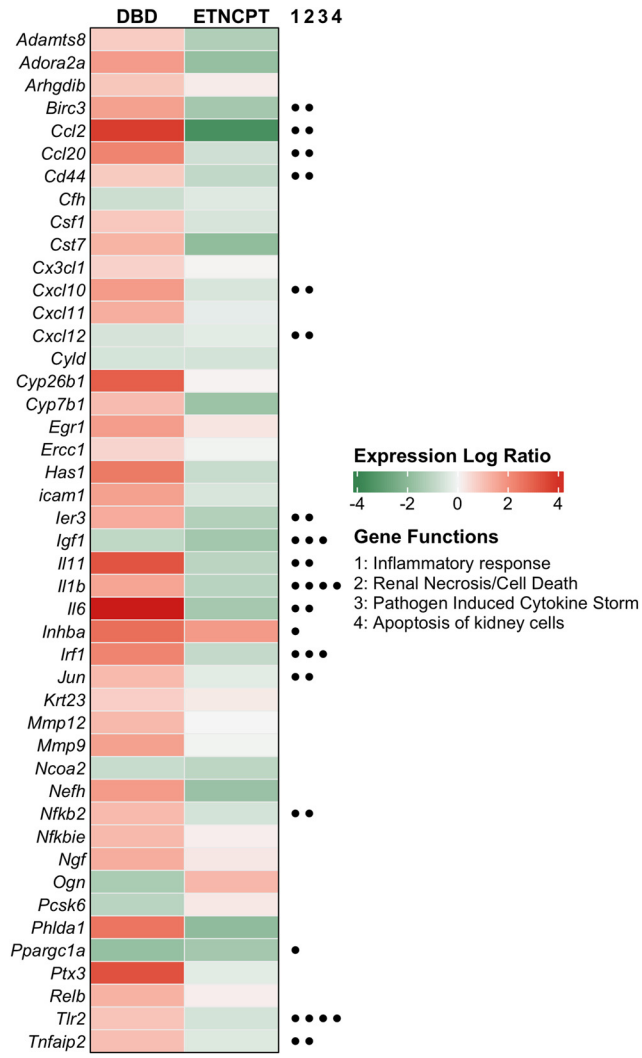

Figure 8. Comparison with a previously established dataset of downstream TNF targets revealed a significant overlap of 45 shared genes. These common target genes display predominantly opposing expression profiles, characterized by inverse $|\log_2$ fold changes$|$ when comparing DBD versus control (CTL) conditions of our previous work against etanercept-treated DBD (ETNCPT) versus CTL conditions of our actual study. DBD, donation after brain death.

comparisons. This goes in line with the transcriptomic identification of suppressed immune cell trafficking and activation functions. IPA analysis predicted significant inhibition of recruitment of phagocytes and recruitment of mononuclear leukocytes. TNFα upregulates expression of chemokines (CCL2 and CCL5) and adhesion molecules (ICAM-1 and VCAM-1), thereby recruiting monocytes and macrophages to inflamed tissues (63, 64). TNFα blockade simultaneously suppresses both direct cytotoxic TNFα signaling and the recruitment of innate immune effector cells (65, 66), a dual mechanism reflected in the broad suppression of inflammatory amplification pathways including IL-6 signaling, cytokine storm signaling, and NF-κB signaling, not achieved by selective antagonism of individual chemokines or adhesion molecules.

Beyond innate immunity, transcriptomic analysis revealed that etanercept profoundly suppressed adaptive immune activation. Lymphocyte proliferation was identified as the most significantly inhibited biological function, with coordinated suppression of B cell proliferation and T cell proliferation. The involvement of 21 key molecules in suppressing lymphocyte proliferation—including Jun, Cxcl12, Map3k7, and Traf2—indicates coordinated downregulation of TNF-dependent immune activation pathways (67, 68). These results demonstrate that TNFα acts as a central hub integrating both innate and adaptive immune responses in the context of brain death-induced kidney injury.

Our work has experimental limitations. First, our assessments were restricted to the donor kidney at 6 h following brain death, without evaluation of transplant outcomes in recipients. Although the substantial reduction in tubular injury, apoptotic events, and acute tubular necrosis represents compelling evidence of organ preservation, improved donor organ quality does not necessarily predict improved graft function in transplant recipients, as recipient-level factors such as alloimmune responses and calcineurin inhibitor toxicity may dominate subsequent graft dysfunction. In addition, renal function was not directly assessed by gold-standard glomerular filtration rate measurements (e.g., inulin or sinistrin clearance), which would have provided a more precise functional characterization of the observed structural protection. Second, our rat model employed isoflurane anesthesia and specific surgical approaches to brain death induction that not fully recapitulate human brain death physiology.

In addition, the inclusion of only three males and three females in the control group limits power to detect subtle sex-specific differences. Although our factorial design allowed formal testing of sex and sex × treatment interaction terms, and no significant interaction was observed, we acknowledge that modest sex-dependent effects may have gone undetected (69, 70). Thus, although the pooled analyses support a robust overall treatment effect, larger studies will be needed to more definitively characterize sex-specific responses.

Clinical translation will require optimization of etanercept dosing, timing relative to brain death declaration, and adaptation for human pharmacokinetics. Finally, the 6-h observation window reflects a practical constraint of the rodent brain death model, as maintaining physiological stability beyond this time point is limited by progressive cardiovascular decompensation (71). This temporal window represents an optimal balance between preserving organ viability and maintaining experimental rigor and aligns with our previous work (12).

In conclusion, our findings converge with recent human genetic evidence and clinical data highlighting TNFα as a central target for donor-directed organ protection. We show that etanercept suppresses the TNFα-driven pathophysiological cascade in brain death kidneys across 2 complementary levels: inhibition of parenchymal apoptosis and prevention of myeloid cell infiltration. These findings directly align with the clinical observation that donors carrying the high-TNF-producing rs3093662 G-allele or exhibiting elevated circulating TNFα levels face an increased risk of late graft loss (59, 60). Taken together, this preclinical-to-clinical continuum suggests that TNFα blockade at the time of brain death may represent a rational donor intervention to improve organ quality at the moment of procurement (23, 72–76). The translation of these donor-level improvements to functional benefits in transplant recipients now requires demonstration

Downloaded from journals.physiology.org/journal/ajprenal at Université de Liège (139.165.031.035) on July 14, 2026.

in a complete rat model of kidney transplantation with assessment of delayed graft function, early graft function, and long-term graft survival. If etanercept-pretreated DBD kidneys demonstrate reduced DGF incidence, improved early graft function, and enhanced long-term allograft outcomes compared with untreated DBD kidneys, this intervention could fundamentally reshape donor management strategies.

DATA AVAILABILITY

Raw count data of RNA sequencing are available online at Figshare: https://doi.org/10.6084/m9.figshare.30987193.

SUPPLEMENTAL MATERIAL

Supplemental Table S1: https://doi.org/10.6084/m9.figshare.32319819.

ACKNOWLEDGMENTS

The authors thank the GIGA Genomics Platform (www.giga.ulg.ac.be) for technical assistance.

GRANTS

T.P.C. and M.N. are Fellows of the Fonds National de la Recherche Scientifique (FNRS), and F.J. and O.D. received support from the FNRS and from the University of Liège (Fonds Spéciaux à la Recherche, Fonds Léon Fredericq).

DISCLOSURES

No conflicts of interest, financial or otherwise, are declared by the authors.

AUTHOR CONTRIBUTIONS

T.P.C., M.V., P.E., O.D., and F.J. conceived and designed research; T.P.C. and J.A. performed experiments; T.P.C. and F.J. analyzed data; T.P.C., P.E., and F.J. interpreted results of experiments; T.P.C. prepared figures; T.P.C. drafted manuscript; T.P.C., P.E., O.D., and F.J. edited and revised manuscript; T.P.C., J.A., M.N., M.V., P.E., O.D., and F.J. approved final version of manuscript.

REFERENCES

1. **Abecassis M**, **Bartlett ST**, **Collins AJ**, **Davis CL**, **Delmonico FL**, **Friedewald JJ**, **Hays R**, **Howard A**, **Jones E**, **Leichtman AB**, **Merion RM**, **Metzger RA**, **Pradel F**, **Schweitzer EJ**, **Velez RL**, **Gaston RS.** Kidney transplantation as primary therapy for end-stage renal disease: a National Kidney Foundation/Kidney Disease Outcomes Quality Initiative (NKF/KDOQITM) conference. *Clin J Am Soc Nephrol* 3: 471–480, 2008. doi:10.2215/CJN.05021107.
2. **Wolfe RA**, **Ashby VB**, **Milford EL**, **Ojo AO**, **Ettenger RE**, **Agodoa LY**, **Held PJ**, **Port FK.** Comparison of mortality in all patients on dialysis, patients on dialysis awaiting transplantation, and recipients of a first cadaveric transplant. *N Engl J Med* 341: 1725–1730, 1999. doi:10.1056/NEJM199912023412303.
3. **Schnuelle P**, **Lorenz D**, **Trede M**, **Van Der Woude FJ.** Impact of renal cadaveric transplantation on survival in end-stage renal failure. *J Am Soc Nephrol* 9: 2135–2141, 1998. doi:10.1681/ASN.V9112135.
4. **Eurotransplant.** 2023 Annual Report (Online), 2024. https://cdn.sanity.io/files/ngz8tmzz/production/24445ce7c521641ca1cd28e24ff7ff2442576fcb.pdf [2026 Jul 1].
5. **European Directorate for the Quality of Medicines & HealthCare.** NEWSLETTER TRANSPLANT: International Figures on Donation and Transplantation, 2023 (Online). European Directorate for the Quality of Medicines & HealthCare, 2024. https://www.transplant-observatory.org/download/newsletter-transplant-2024/ [2025 Jul 11].
6. **Perico N**, **Cattaneo D**, **Sayegh MH**, **Remuzzi G.** Delayed graft function in kidney transplantation. *Lancet* 364: 1814–1827, 2004. doi:10.1016/S0140-6736(04)17406-0.
7. **Erpicum P**, **Pinto Coelho T**, **Bonvoisin C**, **Bouquegneau A**, **Grosch S**, **Navez M**, **Vandermeulen M**, **Beguin Y**, **Detry O**, **Jouret F**, **Weekers L.** [Delayed graft function: an ongoing clinical challenge]. *Rev Med Liege* 78: 107–113, 2023.
8. **Detry O**, **Le Dinh H**, **Noterdaeme T**, **De Roover A**, **Honoré P**, **Squifflet JP**, **Meurisse M.** Categories of donation after cardiocirculatory death. *Transplant Proc* 44: 1189–1195, 2012. doi:10.1016/j.transproceed.2012.05.001.
9. **Pruett TL**, **Martin P**, **Gupta D.** Outcomes of kidneys used for transplantation: an analysis of survival and function. *Front Transplant* 3: 1335999, 2024. doi:10.3389/FRTRA.2024.1335999/BIBTEX.
10. **Li MT**, **Ramakrishnan A**, **Yu M**, **Daniel E**, **Sandra V**, **Sanichar N**, **King KL**, **Stevens JS**, **Husain SA**, **Mohan S.** Effects of delayed graft function on transplant outcomes: a meta-analysis. *Transplant Direct* 9: e1433, 2023. doi:10.1097/TXD.0000000000001433.
11. **Le Dinh H**, **Weekers L**, **Bonvoisin C**, **Krzesinski JM**, **Monard J**, **de Roover A**, **Squifflet JP**, **Meurisse M**, **Detry O.** Delayed graft function does not harm the future of donation-after-cardiac death in kidney transplantation. *Transplant Proc* 44: 2795–2802, 2012. doi:10.1016/j.transproceed.2012.09.087.
12. **Pinto Coelho T**, **Erpicum P**, **Navez M**, **Vandermeulen M**, **Detry O**, **Jouret F.** Kidney transplant injury associated with brain death is mediated by TNFα, independently of renal innervation. *Am J Physiol Renal Physiol* 329: F128–F142, 2025. doi:10.1152/AJPRENAL.00109.2025.
13. **Outwater KM**, **Rockoff MA.** Diabetes insipidus accompanying brain death in children. *Neurology* 34: 1243–1246, 1984. doi:10.1212/WNL.34.9.1243.
14. **Gordon JK**, **McKinlay J.** Physiological changes after brain stem death and management of the heart-beating donor. *BJA Educ* 12: 225–229, 2012. doi:10.1093/bjaceaccp/mks02.
15. **Morganti-Kossman MC**, **Lenzlinger PM**, **Hans V**, **Stahel P**, **Csuka E**, **Ammann E**, **Stocker R**, **Trentz O**, **Kossmann T.** Production of cytokines following brain injury: beneficial and deleterious for the damaged tissue. *Mol Psychiatry* 2: 133–136, 1997. doi:10.1038/sj.mp.4000227.
16. **Schwarz P**, **Custódio G**, **Rheinheimer J**, **Crispim D**, **Leitão CB**, **Rech TH.** Brain death-induced inflammatory activity is similar to sepsis-induced cytokine release. *Cell Transplant* 27: 1417–1424, 2018. doi:10.1177/0963689718785629.
17. **Al-Lamki RS**, **Wang J**, **Vandenabeele P**, **Bradley JA**, **Thiru S**, **Luo D**, **Min W**, **Pober JS**, **Bradley JR.** TNFR1- and TNFR2-mediated signaling pathways in human kidney are cell type-specific and differentially contribute to renal injury. *FASEB J* 19: 1637–1645, 2005. doi:10.1096/fj.05-3841com.
18. **Lee HH**, **Cho YI**, **Kim SY**, **Yoon YE**, **Kim KS**, **Hong SJ**, **Han WK.** TNF-α-induced inflammation stimulates apolipoprotein-A4 via activation of TNFR2 and NF-κB signaling in kidney tubular cells. *Sci Rep* 7: 8856–8859, 2017. doi:10.1038/s41598-017-08785-2.
19. **Wen Y**, **Lu X**, **Privratsky JR**, **Ren J**, **Ali S**, **Yang B**, **Rudemiller NP**, **Zhang J**, **Nedospasov SA**, **Crowley SD.** TNF- from the proximal nephron exacerbates aristolochic acid nephropathy. *Kidney360* 5: 44–56, 2024. doi:10.34067/KID.0000000000000314.
20. **Wang Y**, **Zhang H**, **Chen Q**, **Jiao F**, **Shi C**, **Pei M**, **Lv J**, **Zhang H**, **Wang L**, **Gong Z.** TNF-α/HMGB1 inflammation signalling pathway regulates pyroptosis during liver failure and acute kidney injury. *Cell Prolif* 53: e12829, 2020. doi:10.1111/CPR.12829.
21. **Shi Y**, **Su Y**, **Ge X**, **Li C**, **Meng X**, **Liang Y**, **Chen Y.** Treatment with etanercept attenuates brain death-associated liver injuries in rats. *Int J Clin Exp Med* 12: 6745–6756, 2019.
22. **Choi SW**, **Stiff P**, **Cooke K**, **Ferrara JLM**, **Braun T**, **Kitko C**, **Reddy P**, **Yanik G**, **Mineishi S**, **Paczesny S**, **Hanauer D**, **Pawarode A**, **Peres E**, **Rodriguez T**, **Smith S**, **Levine JE.** TNF-inhibition with etanercept for graft versus host disease prevention in high risk HCT: lower TNFR1 levels correlate with better outcomes. *Biol Blood Marrow Transplant* 18: 1525–1532, 2012. doi:10.1016/j.bbmt.2012.03.013.

Downloaded from journals.physiology.org/journal/ajprenal at Université de Liège (139.165.031.035) on July 14, 2026.

23. **Erpicum P**, **Weekers L**, **Detry O**, **Bonvoisin C**, **Delbouille M-H**, **Grégoire C**, **Baudoux E**, **Briquet A**, **Lechanteur C**, **Maggipinto G**, **Somja J**, **Pottel H**, **Baron F**, **Jouret F**, **Beguin Y.** Infusion of third-party mesenchymal stromal cells after kidney transplantation: a phase I-II, open-label, clinical study. *Kidney Int* 95: 693–707, 2019. doi:10.1016/J.KINT.2018.08.046.
24. **Rowart P**, **Erpicum P**, **Detry O**, **Weekers L**, **Grégoire C**, **Lechanteur C**, **Briquet A**, **Beguin Y**, **Krzesinski JM**, **Jouret F.** Mesenchymal stromal cell therapy in ischemia/reperfusion injury. *J Immunol Res* 2015: 602597, 2015. doi:10.1155/2015/602597.
25. **Zeng J**, **Zhong Q**, **Feng X**, **Li L**, **Feng S**, **Fan Y**, **Song T**, **Huang Z**, **Wang X**, **Lin T.** Conversion from calcineurin inhibitors to mammalian target of rapamycin inhibitors in kidney transplant recipients: a systematic review and meta-analysis of randomized controlled trials. *Front Immunol* 12: 663602, 2021. doi:10.3389/FIMMU.2021.663602/BIBTEX.
26. **Hansen CM**, **Bachmann S**, **Su M**, **Budde K**, **Choi M.** Calcineurin inhibitor associated nephrotoxicity in kidney transplantation—a transplant nephrologist's perspective. *Acta Physiol (Oxf)* 241: e70047, 2025. doi:10.1111/apha.70047.
27. **Hellemans R**, **Bosmans JL**, **Abramowicz D.** Induction therapy for kidney transplant recipients: do we still need anti-IL2 receptor monoclonal antibodies? *Am J Transplant* 17: 22–27, 2017. doi:10.1111/ajt.13884.
28. **Vandermeulen M**, **Erpicum P**, **Weekers L**, **Briquet A**, **Lechanteur C**, **Detry O**, **Beguin Y**, **Jouret F.** Mesenchymal stromal cells in solid organ transplantation. *Transplantation* 104: 923–936, 2020. doi:10.1097/TP.0000000000003077.
29. **Vandermeulen M**, **Erpicum P**, **Bletard N**, **Poma L**, **Jouret F**, **Detry O.** Effect of the combination of everolimus and mesenchymal stromal cells on regulatory T cells levels and in a liver transplant rejection model in rats. *Front Immunol* 13: 877953, 2022. doi:10.3389/fimmu.2022.877953.
30. **Navez M**, **Gilbo N**, **Vandermeulen M**, **Pinto Coelho T**, **Erpicum P**, **Lagny MG**, **Malisoux C**, **Guarin C**, **Thierry G**, **Delanaye P**, **Cavalier E**, **Jouret F**, **Detry O.** Simultaneous ex situ normothermic perfusion of paired kidneys in pigs. *Artif Organs* 49: 1405–1416, 2025. doi:10.1111/AOR.15016.
31. **Hosgood SA**, **Thompson E**, **Moore T**, **Wilson CH**, **Nicholson ML.** Normothermic machine perfusion for the assessment and transplantation of declined human kidneys from donation after circulatory death donors. *Br J Surg* 105: 388–394, 2018. doi:10.1002/BJS.10733.
32. **Dumbill R**, **Knight S**, **Hunter J**, **Fallon J**, **Voyce D**, **Barrett J**, **Ellen M**, **Conroy E**, **Roberts IS**, **James T**, **Allen G**, **Brook J**, **Weissenbacher A**, **Ploeg R**, **Coussios C**, **Friend P.** Prolonged normothermic perfusion of the kidney prior to transplantation: a historically controlled, phase 1 cohort study. *Nat Commun* 16: 4584, 2025. doi:10.1038/S41467-025-59829-5.
33. **Nowlan ML**, **Drewe E**, **Bulsara H**, **Esposito N**, **Robins RA**, **Tighe PJ**, **Powell RJ**, **Todd I.** Systemic cytokine levels and the effects of etanercept in TNF receptor-associated periodic syndrome (TRAPS) involving a C33Y mutation in TNFRSF1A. *Rheumatology (Oxford)* 45: 31–37, 2006. doi:10.1093/RHEUMATOLOGY/KEI090.
34. **Schulz M**, **Dotzlaw H**, **Neeck G.** Ankylosing spondylitis and rheumatoid arthritis: serum levels of TNF-α and its soluble receptors during the course of therapy with etanercept and infliximab. *Biomed Res Int* 2014: 675108, 2014. doi:10.1155/2014/675108.
35. **Wang CW**, **Yang LY**, **Chen CB**, **Ho HC**, **Hung SI**, **Yang CH**, **Chang CJ**, **Su SC**, **Hui RCY**, **Chin SW**, **Huang LF**, **Lin YYW**, **Chang WY**, **Fan WL**, **Yang CY**, **Ho JC**, **Chang YC**, **Lu CW**, **Chung WH**; **the Taiwan Severe Cutaneous Adverse Reaction (TSCAR) Consortium.** Randomized, controlled trial of TNF-α antagonist in CTL-mediated severe cutaneous adverse reactions. *J Clin Invest* 128: 985–996, 2018. doi:10.1172/JCI93349.
36. **Abdelhalim Yameny A**, **Yameny AA.** IL-6, TNF-α, IL-1β, and IFN-γ cytokines as core inflammatory biomarkers: biological roles, diagnostic utility, and clinical applications. *J Biosci Appl Res* 11: 1055–1061, 2025. doi:10.21608/JBAAR.2025.456942.
37. **Gidon A**, **Louet C**, **Røst LM**, **Bruheim P**, **Flo TH.** The tumor necrosis factor alpha and interleukin 6 auto-paracrine signaling loop controls mycobacterium avium infection via induction of IRF1/IRG1 in human primary macrophages. *mBio* 12: e02121, 2021. doi:10.1128/mBio.02121-21.
38. **Caldwell AB**, **Birnbaum HA**, **Cheng Z**, **Hoffmann A**, **Vargas JD.** Network dynamics determine the autocrine and paracrine signaling functions of TNF. *Genes Dev* 28: 2120–2133, 2014. doi:10.1101/GAD.244749.114.
39. **Walter BA**, **Purmessur D**, **Likhitpanichkul M**, **Weinberg A**, **Cho SK**, **Qureshi SA**, **Hecht AC**, **Iatridis JC.** Inflammatory kinetics and efficacy of anti-inflammatory treatments on human nucleus pulposus cells. *Spine (Phila Pa 1976)* 40: 955–963, 2015. doi:10.1097/BRS.0000000000000932.
40. **Bailly S**, **Ferrua B**, **Fay M**, **Gougerot-Pocidalo MA.** Differential regulation of IL 6, IL 1 A, IL 1β and TNFα production in LPS-stimulated human monocytes: role of cyclic AMP. *Cytokine* 2: 205–210, 1990. doi:10.1016/1043-4666(90)90017-N.
41. **Morozova N**, **Avramovič MZ**, **Markelj G**, **Toplak N**, **Avčin T.** Dynamics of serum levels of TNF-α in a longitudinal follow-up study in 98 patients with juvenile idiopathic arthritis treated with anti-TNF-α biological drugs. *Clin Rheumatol* 43: 2287–2293, 2024. doi:10.1007/s10067-024-07012-4.
42. **Liu C**, **Chu D**, **Kalantar-Zadeh K**, **George J**, **Young HA**, **Liu G.** Cytokines: from clinical significance to quantification. *Adv Sci (Weinh)* 8: e2004433, 2021. doi:10.1002/ADVS.202004433.
43. **Watts RP**, **Thom O**, **Fraser JF.** Inflammatory signalling associated with brain dead organ donation: from brain injury to brain stem death and posttransplant ischaemia reperfusion injury. *J Transplant* 2013: 521369, 2013. doi:10.1155/2013/521369.
44. **Yousif AS**, **Ronsard L**, **Shah P**, **Omatsu T**, **Sangesland M**, **Bracamonte Moreno T**, **Lam EC**, **Vrbanac VD**, **Balazs AB**, **Reinecker HC**, **Lingwood D.** The persistence of interleukin-6 is regulated by a blood buffer system derived from dendritic cells. *Immunity* 54: 235–246.e5, 2021. doi:10.1016/J.IMMUNI.2020.12.001.
45. **Ho GYF**, **Xue XN**, **Burk RD**, **Kaplan RC**, **Cornell E**, **Cushman M.** Variability of serum levels of tumor necrosis factor-alpha, interleukin 6, and soluble interleukin 6 receptor over 2 years in young women. *Cytokine* 30: 1–6, 2005. doi:10.1016/j.cyto.2004.08.008.
46. **Murugan R**, **Venkataraman R**, **Wahed AS**, **Elder M**, **Carter M**, **Madden NJ**, **Kellum JA**; **HIDonOR Study Investigators.** Preload responsiveness is associated with increased interleukin-6 and lower organ yield from brain-dead donors. *Crit Care Med*. 37: 2387–2393, 2009. doi:10.1097/CCM.0b013e3181a960d6.
47. **Donado CA**, **Cao AB**, **Simmons DP**, **Croker BA**, **Brennan PJ**, **Brenner MB.** A two-cell model for IL-1β release mediated by death-receptor signaling. *Cell Rep* 31: 107466, 2020. doi:10.1016/J.CELREP.2020.03.030.
48. **Kelley N**, **Jeltema D**, **Duan Y**, **He Y.** The NLRP3 inflammasome: an overview of mechanisms of activation and regulation. *Int J Mol Sci* 20: 3328, 2019. doi:10.3390/IJMS20133328.
49. **Brown J**, **Wang H**, **Hajishengallis GN**, **Martin M.** TLR-signaling networks: an integration of adaptor molecules, kinases, and cross-talk. *J Dent Res* 90: 417–427, 2011. doi:10.1177/0022034510381264.
50. **Liu T**, **Zhang L**, **Joo D**, **Sun SC.** NF-κB signaling in inflammation. *Signal Transduct Target Ther* 2: 17023, 2017. doi:10.1038/sigtrans.2017.23.
51. **Kułdo JM**, **Westra J**, **Àsgeirsdóttir SA**, **Kok RJ**, **Oosterhuis K**, **Rots MG**, **Schouten JP**, **Limburg PC**, **Molema G.** Differential effects of NF-κB and p38 MAPK inhibitors and combinations thereof on TNF-α- and IL-1β-induced proinflammatory status of endothelial cells in vitro. 289: 1229–1239, 2005. doi:10.1152/AJPCELL.00620.2004.
52. **Peda JD**, **Salah SM**, **Wallace DP**, **Fields PE**, **Grantham CJ**, **Fields TA**, **Swenson-Fields KI.** Autocrine IL-10 activation of the STAT3 pathway is required for pathological macrophage differentiation in polycystic kidney disease. *Dis Model Mech* 9: 1051–1061, 2016. doi:10.1242/DMM.024745.
53. **Chanteux H**, **Guisset AC**, **Pilette C**, **Sibille Y.** LPS induces IL-10 production by human alveolar macrophages via MAPKinases- and Sp1-dependent mechanisms. *Respir Res* 8: 71, 2007. doi:10.1186/1465-9921-8-71.
54. **Huynh L**, **Kusnadi A**, **Park SH**, **Murata K**, **Park-Min K-H**, **Ivashkiv LB.** Opposing regulation of the late phase TNF response by mTORC1-IL-10 signaling and hypoxia in human macrophages. *Sci Rep* 6: 1–14, 2016. doi:10.1038/srep31959.
55. **Tummers B**, **Green DR.** Caspase-8; regulating life and death. *Immunol Rev* 277: 76–89, 2017. doi:10.1111/imr.12541.

Downloaded from journals.physiology.org/journal/ajprenal at Université de Liège (139.165.031.035) on July 14, 2026.

56. **Green DR.** The death receptor pathway of apoptosis. *Cold Spring Harb Perspect Biol* 14: a041053, 2022. doi:10.1101/CSHPERSPECT.A041053.
57. **Chang DW**, **Xing Z**, **Pan Y**, **Algeciras-Schimnich A**, **Barnhart BC**, **Yaish-Ohad S**, **Peter ME**, **Yang X.** c-FLIPL is a dual function regulator for caspase-8 activation and CD95-mediated apoptosis. *EMBO J* 21: 3704–3714, 2002. doi:10.1093/emboj/cdf356.
58. **Zhang H**, **Li X**, **Lin L.** Biological functions and clinical implications of CFLAR: from cell death mechanisms to therapeutic targeting in immune regulation. *J Inflamm Res* 18: 4911–4928, 2025. doi:10.2147/JIR.S519885.
59. **Poppelaars F**, **da Costa MG**, **Faria B**, **Eskandari SK**, **Seelen MA**, **Damman J.** Tumor necrosis factor-α gene polymorphism is associated with short- and long-term kidney allograft outcomes. *JIR* 15: 2243–2254, 2022. doi:10.2147/JIR.S334738.
60. **Fawaz S**, **Hartling I**, **Michelakis IE**, **Vaughan RH**, **Ploeg RJ**, **Sharples E**, **Charles PD**, **Kaisar M.** Circulating tumor necrosis factor α in deceased donors promotes kidney injury and associates with inferior short- and long-term graft function and survival. *Am J Transplant* 26: 1390–1403, 2026. doi:10.1016/j.ajt.2026.01.023.
61. **Lim S**, **Ryu J**, **Shin JA**, **Shin MJ**, **Ahn YK**, **Kim JJ**, **Han KH.** Tumor necrosis factor-α potentiates RhoA-mediated monocyte transmigratory activity in vivo at a picomolar level. *ATVB* 29: 2138–2145, 2009. doi:10.1161/ATVBAHA.109.195735.
62. **Gschwandtner M**, **Derler R**, **Midwood KS.** More than just attractive: how CCL2 influences myeloid cell behavior beyond chemotaxis. *Front Immunol* 10: 2759, 2019. doi:10.3389/FIMMU.2019.02759.
63. **Xia P**, **Gamble JR**, **Rye KA**, **Wang L**, **Hii CST**, **Cockerill P**, **Khew-Goodall Y**, **Bert AG**, **Barter PJ**, **Vadas MA.** Tumor necrosis factor-α induces adhesion molecule expression through the sphingosine kinase pathway. *Proc Natl Acad Sci USA* 95: 14196–14201, 1998. doi:10.1073/pnas.95.24.14196.
64. **Deshmane SL**, **Kremlev S**, **Amini S**, **Sawaya BE.** Monocyte chemoattractant protein-1 (MCP-1): an overview. *J Interferon Cytokine Res* 29: 313–326, 2009. doi:10.1089/jir.2008.0027.
65. **Yu H**, **Lin L**, **Zhang Z**, **Zhang H**, **Hu H.** Targeting NF-κB pathway for the therapy of diseases: mechanism and clinical study. *Signal Transduct Target Ther* 5: 209–223, 2020. doi:10.1038/S41392-020-00312-6.
66. **Van Hauwermeiren F**, **Vandenbroucke RE**, **Libert C.** Treatment of TNF mediated diseases by selective inhibition of soluble TNF or TNFR1. *Cytokine Growth Factor Rev* 22: 311–319, 2011. doi:10.1016/j.cytogfr.2011.09.004.
67. **Guo Q**, **Jin Y**, **Chen X**, **Ye X**, **Shen X**, **Lin M**, **Zeng C**, **Zhou T**, **Zhang J.** NF-κB in biology and targeted therapy: new insights and translational implications. *Signal Transduct Target Ther* 9: 53–37, 2024. doi:10.1038/S41392-024-01757-9.
68. **Meixner A**, **Karreth F**, **Kenner L**, **Wagner EF.** JunD regulates lymphocyte proliferation and T helper cell cytokine expression. *EMBO J* 23: 1325–1335, 2004. doi:10.1038/sj.emboj.7600133.
69. **Diester CM**, **Banks ML**, **Neigh GN**, **Negus SS.** Experimental design and analysis for consideration of sex as a biological variable. *Neuropsychopharmacology* 44: 2159–2162, 2019. doi:10.1038/S41386-019-0458-9.
70. **Phillips B**, **Haschler TN**, **Karp NA.** Statistical simulations show that scientists need not increase overall sample size by default when including both sexes in in vivo studies. *PLoS Biol* 21: e3002129, 2023. doi:10.1371/journal.pbio.3002129.
71. **van der Hoeven JAB**, **Molema G**, **Ter Horst GJ**, **Freund RL**, **Wiersema J**, **van Schilfgaarde R**, **Leuvenink HGD**, **Ploeg RJ.** Relationship between duration of brain death and hemodynamic (in)stability on progressive dysfunction and increased immunologic activation of donor kidneys. *Kidney Int* 64: 1874–1882, 2003. doi:10.1046/J.1523-1755.2003.00272.X.
72. **Khbouz B**, **Lallemand F**, **Cirillo A**, **Rowart P**, **Legouis D**, **Sounni NE**, **Noël A**, **De Tullio P**, **de Seigneux S**, **Jouret F.** Kidney-targeted irradiation triggers renal ischemic preconditioning in mice. *Am J Physiol Renal Physiol* 323: F198–F211, 2022. doi:10.1152/ajprenal.00005.2022.
73. **Erpicum P**, **Detry O**, **Weekers L**, **Bonvoisin C**, **Lechanteur C**, **Briquet A**, **Beguin Y**, **Krzesinski JM**, **Jouret F.** Mesenchymal stromal cell therapy in conditions of renal ischaemia/reperfusion. *Nephrol Dial Transplant* 29: 1487–1493, 2014. doi:10.1093/ndt/gft538.
74. **Erpicum P**, **Rowart P**, **Poma L**, **Krzesinski JM**, **Detry O**, **Jouret F.** Administration of mesenchymal stromal cells before renal ischemia/reperfusion attenuates kidney injury and may modulate renal lipid metabolism in rats. *Sci Rep* 7: 8687, 2017. doi:10.1038/s41598-017-08726-z.
75. **Detry O**, **Jouret F**, **Erpicum P**, **Delens L**, **Grégoire C**, **Briquet A**, **Weekers L**, **Baudoux E**, **Lechanteur C**, **Beguin Y.** [Cellules stromales mésenchymateuses et transplantation d'organes]. *Rev Med Liege* 69: 53–56, 2014.
76. **Khbouz B**, **Rowart P**, **Poma L**, **Dahlke E**, **Bottner M**, **Stokes M**, **Bolen G**, **Rahmouni S**, **Theilig F**, **Jouret F.** The genetic deletion of the dual specificity phosphatase 3 (DUSP3) attenuates kidney damage following ischemia/reperfusion injury in mouse. *Acta Physiol (Oxf)* 234: e13735, 2021. doi:10.1111/Apha.13735.

Downloaded from journals.physiology.org/journal/ajprenal at Université de Liège (139.165.031.035) on July 14, 2026.